DEUTSCHES ELEKTRONEN-SYNCHROTRON DESY

DESY SR-72/12
July 1972

The Spectra of the Xenon Fluorides XeF_2 and XeF_4 in the Far UV-Region

by

F. J. Comes, R. Haensel, U. Nielsen, and W. H. E. Schwarz

2 HAMBURG 52 · NOTKESTIEG 1

To be sure that your preprints are promptly included in the HIGH ENERGY PHYSICS INDEX, send them to the following address (if possible by air mail):

DESY
Bibliothek
2 Hamburg 52
Notkestieg 1
Germany

The Spectra of the Xenon Fluorides XeF_2 and XeF_4 in the Far UV-Region

F.J. Comes[+], R. Haensel[++], U. Nielsen[++], and W.H.E. Schwarz[+++]

Deutsches Elektronen-Synchrotron DESY, Hamburg, Germany

The absorption of gaseous and solid XeF_2 and XeF_4 has been measured in the region of 50 to 160 eV. It was possible to reproduce the absorption line shapes observed between 61 and 73 eV by semiempirical calculations based on the one center - one electron - model. According to these results the observed lines could be assigned to transitions from 4d and 4p Xe subshells into 5p, 6s, 6p and 7p levels. The spin orbit splitting of the molecular 4d level has been found to be almost equal to the free atom case. For the first time a ligand field splitting of core levels is observed. In addition to this spin orbit and ligand field splitting are measured to occur in the upper levels. The 4d→5p transition in XeF_4 suggests a dynamic Jahn-Teller-effect.

The gross structure of the spectra in both phases is practically identical for both XeF_2 and XeF_4. The absorption lines of the Rydberg transitions are strongly broadened in the spectra of the solidified gases.

[+] Institut für Physikalische Chemie der Universität Bonn, Bonn, Germany

[++] II. Institut für Experimentalphysik der Universität Hamburg, Hamburg, Germany

[+++] Lehrstuhl für Theoretische Chemie der Universität Bonn, Bonn, Germany

1. INTRODUCTION

Since their first preparation in 1962[1] xenon fluorides have been extensively investigated. Much of the early work up to 1965 has been reviewed in Ref.s[2,3]. The molecular structure in gaseous, and the crystal lattice structure in solid XeF_2 and XeF_4 as well as the nature of the chemical bond have been studied by means of IR spectroscopy[2,4], and by X-ray[5], electron[2] and neutron[2,6] diffraction measurements. The conclusions from these measurements were that the XeF_2 molecule is a F-Xe-F linear chain with a Xe-F distance of 2.14 Å, the XeF_4 molecule a square-planar with a Xe-F distance of 1.92 Å. The XeF_2 solid is tetragonal with the molecular axis parallel to the crystal lattice c-axis (c = 6.99 Å, a = 4.315 Å); XeF_4 forms a monoclinic crystal (a = 5.03 Å, b = 5.92 Å, c = 5.79 Å, $\beta = 99^{o}27'$).

The optical absorption spectrum[2,7] of XeF_2 is characterized by two broad valence shell absorption bands (at 5.3 eV and 7.85 eV) accompanied by a series of sharp bands. No vibrational structure has been resolved. The sharp bands are assigned as Rydberg states and Rydberg formulae for the two expected series are given. In XeF_4 a few high intensity electronic transitions (at 5.3 eV, 6.8 eV, and 9.4 eV) and some weaker bands are observed.

Whereas optical absorption measurements incorporate transitions from the highest occupied molecular orbitals (HOMO's) into the lowest empty ones (LEMO's) UV-photoelectron spectra[8] are concerned with transitions from the HOMO's into the ionization continuum. They can be of some help in

the interpretation of optical absorption spectra although there is much complication due to the strong exchange coupling between the initial and final one-electron levels.

When using high energy radiation, however, the situation is different from the optical case. Transitions from deep lying AO's into the empty MO's occur leading to spectra which are very different from the optical spectra. This is due to the fact that now only weak coupling between the initial and final one-electron states occurs contrary to the phenomena at lower energies where large singlet-triplet splittings are observed. Besides Rydberg states, which are describable in the one-electron approximation, the observed transitions in optical spectra of gaseous compounds can, to a minor extent, be used for the interpretation of the results obtained with high energy photons.

Furthermore, the optical spectra are very complicated due to the transitions from the numerous upper filled molecular orbitals into empty orbitals. The possible assignment of the transitions observed is, therefore, difficult and in no way unambiguous[9]. The various possibilities are, at first sight, very much reduced if high energy photons are absorbed. Neglecting splitting effects, the initial state here is a single atomic orbital. Absorption spectra in the extreme ultraviolet should, therefore, be more simple in structure and should give clear evidence not only of the lowest empty molecular orbital (LEMO) but also of the higher molecular Rydberg orbitals. Whereas in these spectra the initial one-electron level can, in all cases, be identified with certainty there are, in practice, fewer restrictions as compared to the optical spectrum. For example, the d-AO's in the molecular core are nearly m-degenerate. We do not, therefore,

expect a lower number of absorption lines in the high energy spectra, but the lines will be arranged in a much clearer scheme. Compared to x-ray photoelectron spectroscopy (ESCA)[10] better information on the splitting of the initial level caused both by spin orbit coupling and the ligand field of the fluorine atoms can be expected from these absorption spectra.

In solid state spectroscopy the situation is different. The coupling phenomena are much less pronounced so that the one-electron description is a valuable approximation. Direct comparison of the spectra in the far and near uv is thus possible.

On the following pages we will discuss the spectra of XeF_2 and XeF_4 both in the gaseous and solid phase. The measurement shows that the change in absorption properties by solidifying the gaseous probe is only small and apart from minor changes in peak position mainly affects transitions to Rydberg levels. Due to the large extension of the electron distribution in this case the orbitals are affected by the nearest neighbours and thus lead to a pronounced broadening of the corresponding absorption lines.

In Chapter 3 the experimental results, observed when using synchrotron radiation in the region of the 4d and 4p absorption of Xe, are described. In this energy range synchrotron radiation is an ideal source for spectroscopic measurements. Earlier observations on Xe[11] were helpful for understanding the xenon fluoride spectra. Detailed experimental results are given for both XeF_2 and XeF_4 in the gaseous and the solid phase. A theoretical explanation of the experimental findings for the various structures of the observed spectra then follows in Chapter 4. This is done in Chapter

4.2 for transitions into the LEMO of XeF_2 and XeF_4, and in Chapters 4.3 and 4.4 for transitions into the lowest Rydberg orbitals. Spin orbit coupling and ligand field effects are discussed here. For the first time a splitting of inner orbitals due to the asymmetric part of the ligand field is observed.

2. EXPERIMENTAL PROCEDURE

2.1 General Setup

The absorption measurements were performed using the 7.5 GeV electron synchrotron DESY as the radiation source[12]. The experimental setup is shown in Fig. 1. The light comes from the orbiting electrons in the synchrotron (EO) and passes through a ∿40m long beam pipe. After reflection on a plane mirror (GPM) the light passes the sample chamber which is equipped with gas cell (GC) and cryostat (CR). Finally, a concave mirror (CM) focuses the light into the entrance slit of a grazing incidence 1 m Rowland monochromator. For the measurement a gold coated grating (G) with 2400 lines/mm (blaze angle 4°16', angle of incidence 12°30') was used in first order. The wavelength resolution of the instrument was 0.1 Å over the whole energy range. The detector (PM), a Bendix M 306 open magnetic electron multiplier, was mounted behind the exit slit. The multiplier signal was fed into a 25 Hz lock-in-amplifier (PAR 122) as the light passed a 25 Hz chopper wheel (CH) mounted in the beam pipe. The signal from the monochromator was divided by a monitor signal proportional to the current in the accelerator, thus compensating current fluctuations. The ratio signal was then fed into the Y channel of a XY potentiometric recorder. The X axis of the recorder received voltage from a potentiometer linked to the wavelength drive of the monochromator.

2.2 Gas Cell

A gas cell (GC) could be moved into the beam for absorption measurements of gaseous XeF_2 and XeF_4 (Fig. 2). It was a stainless steel tube, usually 100 mm long, with Al or C windows (1000 Å thick) on both ends. The windows were

10x5 mm^2 and were mounted on highly transparent coppermeshes. The length of the gas cell could be modified between 20 and 500 mm by means of special window supports. The XeF_2 and XeF_4 samples were obtained from Peninsular Chemical Research.

The samples were filled into a sample container (SC) before measuring and were purified by enhanced pumping with an external pumping system for about an hour. If the pumping was insufficient extrastructure due to XeF_2 and Xe could be observed in the spectrum of XeF_4 (other authors have reported similar observations[8]). No further cleaning requirements were necessary.

During measurements the desired pressure was regulated by a valve between the gas cell and the external pumping system. The pressure was measured by a mechanical membrane vacuum manometer (W&T aneroid, 0.1 to 20 Torr). Good correlation and reproducibility between pressure and optical absorptivity were obtained with this instrument; other systems such as electric differential pressure membrane vacuum meters could not be used because of obvious contamination and detuning effects.

While measuring the pressure in the cell was varied between 0.1 and 2 Torr. At these pressures the absorption cell exhibited a transmission from 10 to 50 % for the different regions of the spectrum. If the transmission is too low (pressure too high) the influence of stray light and light from higher orders of the grating causes errors. As the absorption varied a great deal over the investigated energy range measurements at different pressures had to be made to obtain uniform accuracy and to check the consistency of the results. In so doing an overall accuracy of the final absorption values of better than 20 % was obtained. The relative accuracy in adjacent regions

is much better: structures were easily observed if the change in the absorption coefficient exceeded 1 %.

The wavelength calibration[13] was possible by passing Xe into the gas cell from a pressurized bottle connected to the system. The energy calibration was accurate to 0.1 eV.

2.3 Cryostat

A cryostat (CR) was also mounted in the sample chamber to enable absorption measurements of thin films of solid XeF_2 and XeF_4 (Fig. 2). The pressure in the sample chamber was $\sim 10^{-6}$ Torr before sublimation. The temperature of the cryostat was kept at about 80° K. At this temperature XeF_2 and XeF_4 could easily be sublimed, but not their dissociation products Xe and F_2. Thus contamination of the samples by dissociation products was no problem. The sample was surrounded by a cooling shield with tubular extensions to avoid contamination by water vapour. By these means no contamination was observed during the measurements which, on an average, took an hour. The samples were evaporated by admitting gaseous XeF_2 or XeF_4 from the external sample container onto the cooled foil. Purification before the measurements was also carried out by pumping through the open valve into the warm cryostat.

Both the pressure in the gas cell and the thickness of the solid on the cooled support were controlled so as to yield an optimal signal. No direct measurements of the thickness have been made. But it can be estimated from the continuous absorption in the range of 70 - 150 eV, where both the solid and the gas phase are expected to have the same integrated absolute cross section. Typical values were of the order of several hundred Å.

The Al and C foils serving as substrates in the cryostat and as windows in the gas cell were used according to the energy range. Al was used for the measurements up to 70 eV where Al begins to absorb strongly[14], thus suppressing higher order light below 70 eV. C foils were used above 70 eV. Here the higher order light was effectively suppressed by adjusting the angle of incidence of the grating so (namely 12°30') that no light above 180 eV was reflected.

By simultaneous use of the cryostat and gas cell very precise measurements of the relative energy positions of corresponding lines in gaseous and solid samples were performed.

2.4 Data Handling

The data obtained with the XY recorder were digitalized, punched onto cards and computerized to give an average absorption curve for all measurements.

3. EXPERIMENTAL RESULTS

3.1 General Behaviour of the Absorption Curves

Figures 3 and 4 show the absorption spectra of gaseous (upper part) and solid (lower part) XeF_2 and XeF_4, respectively, in the energy range 50 eV to 160 eV. In all four curves we can distinguish 5 regions of characteristic absorption features:

Region a: On the low energy side we observe an absorption continuum with decreasing cross-section going to higher energies due to transitions from the outer shells.

Region b: Near 60 eV we see two (in XeF_2) or three (in XeF_4) intensive broad peaks which, due to energy reasons, have to be assigned to the onset of 4d transitions.

Region c: At higher energies we find additional absorption lines having a much smaller half-width than those in region b. This structure is not observed in solid XeF_4.

Region d: Near 70 eV we observe the onset of a broad continuum with its maximum near 95 eV.

Region e: On the high energy side of the broad maximum near 145 eV we observe a small single peak, except for solid XeF_4, which is due to excitation of the Xe 4p shell in accordance with observations in Xe.

3.2 Continuum Absorption

3.2.1 Region a

The continuous absorption on the low energy side of the spectrum decreases with increasing photon energy until nearly 70 eV where a second continuum occurs. Below 70 eV the absorption is ascribed to a transition from the

outer shells.

It is interesting to compare the continuous absorption of XeF_2 and XeF_4 with that of Xe (Fig.s 3-4). Whereas in Xe the absorption cross-section before the 4d onset is ∿2 Mb, it is much higher in XeF_2 (∿22±2 Mb) and XeF_4 (∿25±2 Mb). As the absorption is due to outer shell transitions we have to take the absorption of two F atoms in XeF_2 and of four F atoms in XeF_4 into consideration. If we inspect the absorption spectra of the four rare gases Ne, Ar, Kr, and Xe[18], we see that for Ar, Kr, and Xe the oscillator strength for transitions from the valence shell is exhausted near 60 eV. In contrast to this the absorption of neon at 60 eV has still nearly the same value (∿10 Mb) as near the ionization limit. Absorption extends over a wide energy range. Consequently, only 25 % of the oscillator strength is exhausted near 60 eV; a value of 100 % is not reached before 300 eV.

These rare gas data are in accordance with theoretical calculations made by McGuire[15]. The calculations show that the absorption of Ne and F is similar. We, therefore, conclude that F has a much higher absorption cross-section than Xe near 60 eV which explains the increase in the absorption cross-section going from Xe to XeF_2 and XeF_4.

3.2.2 Region d

The broad maximum above 70 eV is rather similar in shape and height to that observed in Xe[11]. If we subtract the contribution of the valence shells the remaining absorption is nearly identical to the continuous absorption spectrum of Xe. We explain the absorption in region d as being caused by the delayed onset of $4d \rightarrow \varepsilon f$ transitions. The number of effec-

tive electrons N_{eff} whose oscillator strength is exhausted within the energy range of our measurements (defined by

$$N_{eff} = \frac{mc\ A}{\pi\ e^2\ Lh\rho} \int_{E_1}^{E_2} \alpha\ n\ dE$$

with the Arogadro number L, atomic weight A, density ρ and the real part of the refractive index n, which is set equal 1 in the energy range under discussion) is about 11 between E_1 = 70 eV and E_2 = 150 eV. This is in good agreement with the number of 10 electrons contained in the Xe 4d subshell and is the same experimental result for both gaseous and solid XeF_2 and XeF_4 as it was the case for pure Xe in both states of aggregation.

3.3 Fine Structure near the Xe 4d Threshold (Region b and c)

3.3.1 Molecules

Figures 5 and 6 show the fine structure in gaseous XeF_2 and XeF_4 in the energy region between 60 eV and 75 eV. The details of region c for XeF_2 (66 eV to 73 eV) are given in Fig. 7 and for XeF_4 (69 eV to 72 eV) in Fig. 8. Table I (XeF_2) and Table II (XeF_4) contain the energy values for the peak maxima. The labelling of each peak is explained in Chapter 4.

We can easily see the characteristic differences of the features below 66 eV (region b) and above (region c).

The absorption structures in region b are typical for the fluorides and have no analogues in the Xe spectrum. The energy separation between the two peaks O_{23} and O_{45} in XeF_2 is 1.91 eV which is very near the value of 1.97 eV of the spin orbit splitting of the Xe 4d level. This strongly suggests that the two peaks are spin orbit mates. Similar splitting is observed in

the case of XeF_4. In the region b of its spectrum two pairs of peaks occur with separation $\Delta E(O_{23}, O_{45}) = 2.2$ eV and $E(O'_{123}, O'_{45}) = 1.8$ eV.

Contrary to the region b the absorption lines in the region c correspond to 4d-Rydberg transitions of Xe. Their onset is shifted to higher energies by the amount of +2.5 eV for XeF_2 and +5 eV for XeF_4. This roughly compares with the chemical shifts of the 4d levels of these compounds as measured by means of ESCA[10]. The smaller number of peaks observed in the XeF_4-spectrum is attributed to experimental reasons. As we proceed from Xe to XeF_2 and XeF_4 the intensity of the peaks in region c decreases so that the transitions of low intensity are suppressed. One peak (C_5) very near the Al $L_{II,III}$ absorption edge was not reproducible.

3.3.2 Solids

Considering the corresponding fine structure in solid XeF_2 and XeF_4 (Fig.s 5 and 6) we see that the main character of the structures is preserved. The doublet O_{23}, O_{45} in gaseous XeF_2 is shifted by 0.42 eV, 0.35 eV to lower energies; the structures in XeF_4 are shifted even less (0.17 eV, 0.15 eV, 0.02 eV, ~0.0 eV). The similar position and intensity distribution of these peaks suggest transitions to the low-lying molecular orbital already discussed which is scarcely affected in the solid.

Larger differences can be noted for region c: the fine structure in XeF_2 is broadened and the three peaks at 69.2, 71.1, and 72.8 eV are hard to recognize. This is in accordance with their interpretation as being caused by transitions into Rydberg states. They are shifted to higher energies as compared to the position of the structure in the gaseous case by about 1.5 eV. In solid XeF_4 fine structure in region c is no

longer observable. This is to be expected because these transitions already led to rather weak absorption lines for the gaseous compounds. We may conclude from these observations that solidification does not essentially influence the first pronounced peak in region b in contrast to the behaviour in region c, because the first peaks are due to more localized transitions, whereas the higher energy peaks are due to transitions into states which are strongly influenced by the next neighbours in the solid.

3.4 Fine Structure near the Xe 4p Threshold at 145 eV (Region c)

As we see from Fig.s 3 and 4 a single peak α appears at 144.91 eV in gaseous XeF_2 and at 147.79 eV in gaseous XeF_4. In solid XeF_2 the peak occurs at ~145 eV whereas there is no detectable absorption structure in solid XeF_4, a feature very similar to the observation in the case of the 4d Rydberg transitions. If we again compare the energy position with that of pure Xe (142 eV)[11] we note a considerable shift towards higher energies. The measured shift of +2.9 eV for XeF_2 and of +5.8 eV for XeF_4 as compared with its position in Xe is in agreement with ESCA measurements[10] on the chemical shift of the 4p level of Xe.

4. Discussion of the Results

The aim of the following discussion is to correlate the observed absorption structures with the molecular orbitals of the xenon fluorides and to present calculations in order to match the measured intensities on the basis of a one-electron model. As the initial 4p and 4d levels of Xe lie rather deep in the core one may expect the interaction of the excited electron with the corresponding hole to be weak and the effect of singlet-triplet splitting of the excited N-electron states to be negligible. As experimental evidence for this we take the findings of Madden and Codling[13] who observed no splitting in the Xe absorption spectrum. Furthermore, theoretical estimations on this intermediate coupling case predict splittings of the molecular states in question, which are smaller than 0.1 eV in almost all cases. Thus we assume that the energy of the N-electron states can be obtained at least within some 1/100 eV from suitable chosen one-electron energies.

The xenon fluorides may be considered in the case of XeF_2 as a stretched F_2 molecule or, in the case of XeF_4, as two stretched F_2 molecules arranged crosswise each with the heavy xenon atom in the center. The influence of the fluorine ligands on the occupied 4p and 4d atomic levels of the free Xe atom will cause a splitting. There is, furthermore, an influence of the fluorine atoms on the empty MOs. As known from ESCA measurements[10] and confirmed by ab initio calculations[9] each F_2 entity in the xenon fluorides bears roughly one negative charge. This means that the empty anti-bonding 2p σ_u-MO of the free F_2 molecule will mix strongly with the occupied $5p_o$ Xe-AO, which is also of anti-bonding character for electrostatic reasons. Consequently, the main component of the LEMO in the xenon fluorides will be the $5p_o$ Xe-AO with some contribution from the 3 σ_u-F_2-MO. The lowest energy

transitions to be expected in the present molecular spectra will be the Xe 4d→"5p" transitions (signed with "O" in Fig.s 3-6).

Because of the Laporte Rule no corresponding 4p→5p transition with any appreciable intensity will be observed. The peaks called α, A,B, ... are, therefore, associated with transitions from 4p or 4d into the next higher empty MO's. As the fluorine atoms are negatively charged the virtual F-AO's are energetically unfavourable. This situation is reversed in the case of the Xe (n=6)-AO's because the Xe atom has an effective charge of almost two atomic units or more in the excited molecule. The final states of the transitions leading to α,A,B ... will, therefore, be associated with Xe Rydberg AO's, the degenerate ones being split by the fluorine ligand field.

4.1 The Core Levels

The 4p and 4d Xe levels are split by two effects: spin orbit interaction and fluorine ligand field perturbation.

As the Xe core orbitals are not expected to be delocalized (or contracted) to any perceptible extent in the process of Xe-F bond formation, the spin orbit interaction can be described by the known spin orbit coupling constant of the free xenon atom (λ_{4d} = 1.97 eV[13] ; λ_{4p} = 12.5 eV [10]). The subsequent results show that the effective molecular spin orbit coupling is only smaller, at the most, by a few 0.01 eV, which is within the persumable reliability of our model.

The only information on the extent of ligand field splitting may be drawn from the recently published non-relativistic ab initio GO-SCF calculations

on the xenon fluorides by Basch et al.[9]. The authors calculated chemical shifts of the centers of gravity of the 4d (4p) levels in XeF_2 and XeF_4 in relation to those of the free xenon atom. The results are 4.20 (4.18) eV and 8.79 (8.75) eV, respectively. The chemical shifts measured by photoelectron spectroscopy[10] are given by 2.95 ± 0.13 eV and 5.47 ± 0.18 eV. They are lower by factors of 0.7 (XeF_2) and 0.625 (XeF_4). This has to be attributed to the single configuration and the not-near-Hartree-Fock character of the computation and also to the limitations of Koopmans' theorem. It is, therefore, worth scaling the calculated ligand field splittings by the above mentioned factors. This results in the numbers given in Fig. 9. The axis, to which the magnetic quantum numbers of the 4d and 4p orbitals refer, is the C_∞ of the $D_{\infty h}$-XeF_2 and the C_4 of the D_{4h}-XeF_4, respectively. We should mention that the calculated splitting pattern is of the order which can be expected from an electrostatic model. The energetically lowest of the d^9-hole states is the one which has its maximum hole density nearest to the negatively charged fluorine atoms.

We now approximate the effective one-electron hamiltonian for the description of the 4d-hole states by

$$H = H_o - \frac{-2\lambda}{5} \underline{L}\,\underline{S} + V_{lig}$$

Here H_o is the totally symmetric part of H. As the first order mixing of orbitals of different symmetry is caused by the rather small ligand field and as the other orbitals are different in energy by more than 50 or 100 eV, it is sufficient to use only the 4d spin-orbitals as basis functions. The hamiltonian matrix for XeF_2 in a basis also suitable for XeF_4 has the following form:

$$
\begin{array}{c|ccccc}
 & & & & & \\
d_0\alpha & E_o-2\delta' & \sqrt{6}/5\cdot\lambda & 0 & 0 & 0 \\
d_1\beta & \sqrt{6}/5\cdot\lambda & E_o-\lambda/5-\delta & 0 & 0 & 0 \\
d_1\alpha & 0 & 0 & E_o+\lambda/5-\delta & 2/5\cdot\lambda & 0 \\
d_2\beta & 0 & 0 & 2/5\cdot\lambda & E_o-2/5\cdot\lambda+\delta+\delta' & 0 \\
d_{-2}\beta & 0 & 0 & 0 & 0 & E_o+2/5\cdot\lambda+\delta+\delta'
\end{array}
$$

This leads to relative values of the eigenvalues and to eigenfunctions given in Fig. 10, and Table III, respectively. The lower indices of the five d_i symbols are also used for the designation of the measured peaks: they distinguish between transitions from different initial to the same final level. Siegbahn et al.[10] measured the absolute energies of the two groups of 4d-levels in XeF_2 and found them to be 70.5 ± 0.2 and 72.5 ± 0.2 eV. If we identify the center of gravity of the measured photoelectron spectra with $\langle H_o \rangle = E_o$ from Fig. 10 we obtain the one-electron energy values given in Table III.

In the case of XeF_4 the hamiltonian matrix is quite similar except for the small non-zero element $H_{45} = \frac{\Delta}{2}$. The level splitting is shown in Fig. 11. The energy values in Table IV relate to Siegbahn's[10] ionization potentials (73.0 and 75.0 eV).

In the case of the 4p hole, where the influence of the spin-orbit coupling is much larger than that of the ligand field, one obtains the splitting pattern of Fig. 12. According to the observed chemical shifts[10], the following level energies are adopted:

	XeF_2	XeF_4	Xe
$4p_1$	148.4	150.9	145.5
$4p_2$	148.6	151.1	
$4p_3$	161.	163.5	158.

4.2 The 4d→5p-Transitions in XeF_2 and XeF_4

4.2.1 The 4d→5p($7\sigma_u$)-Transition in XeF_2

The transitions from 4d into the antibonding orbital 5p($7\sigma_u$) lead to the following characteristics of the observed spectrum (Fig. 5):

1. Two peaks, O_{23} and O_{45}, are recorded.
2. These bands are rather broad, with a mean half-width of 0.9 eV.
3. Band O_{45} is broader by 0.2 eV than band O_{23}.
4. Band O_{45} shows a weak but significant asymmetry.
5. The gap between the two maxima is 1.91 eV, somewhat less than the free atom spin-orbit splitting.
6. The intensity ratio of the bands is 1.2 : 1.
7. The center of gravity corresponds to E_o = 62.21 eV.

All these details can be well understood on the basis of the proposed model:

1. Several of the transitions into non-bonding Rydberg orbitals have widths of only 0.2 - 0.25 eV. We take this value as an upper limit of the natural width of the d^9-hole state of the core (this is expected to be caused mainly by Auger effect). As the upper 5p $7\sigma_u$-level of the transition discussed here has an antibonding character, we expect only two broad, non-resolved vibrational bands with

also a non-resolved ligand field splitting of the $4d_{5/2} \rightarrow 5p$ and $4d_{3/2} \rightarrow 5p$-transitions (point 1).

2. Assuming the force constant of a vibrating molecule to be approximately the same for the ground and the excited state, with the equilibrium distance changed by the amount of Δ, the Franck-Condon factors would lead to the following intensity distribution

$$E = \omega(n + \frac{1}{2}) \qquad I = \frac{(\frac{M}{4}\omega\Delta^2)^n}{n!} \qquad (1)$$

In order to apply this to the symmetrical stretching vibration of XeF_2 (ω = 555 K)[22] we need a reasonable value for Δ. The bond expansion of XeF_2 caused by the anti-bonding σ_u-electron is supposed to be comparable to the bond expansion of the F_2-molecule on formation of σ_u-F_2^- which is about $1a_o$[21]. With this choice of Δ one obtains an intensity distribution which is similar to a Gaussian of half-width 0.75 eV (point 2).

3. This width should be the same for each of the $d_i \rightarrow 5p$ transitions. But instead , the two peaks O_{23} and O_{45} are different in half-widths (point 3); this reflects the different ligand field splitting of the d_2, d_3 and d_4, d_5 level pairs.

4. For further discussion some estimations for the electronic transition moments are needed. To a high degree the five d_i-orbitals will all be pure d-type orbitals with the same radial part. As a first approximation we treat the final 7σ-orbital as a Xe p-orbital. One then obtains the relative intensities as given in Table III. The asymmetry of band O_{45} (point 4) is caused by a weak shoulder on its low energy side.

5. From the calculation a distance of 1.95 eV for the center of gravity of the upper and lower two allowed transitions is obtained. This value is smaller than that of the free atom (point 5) which one obtains by assuming $V_{lig} = 0$. But it is larger than the measured value of 1.91 eV, indicating that the effective spin-orbit coupling in the molecule is reduced by not more than 2 %.

6. V_{lig} not only lowers the effective spin-orbit coupling but also the intensity ratio below a value of 1.5 : 1 (point 6). The intensities of Table III obtained for the ligand field assumed lead to a ratio of 1.4 : 1. Although the measured ratio is 1.2 : 1, one must not expect the ligand field to be much larger. It would otherwise be difficult to interpret the Rydberg spectrum (see below). One should rather take into account that a small electrostatic interaction between the d-hole and the σ_u-electron will have much larger effect on the intensities than on the energy levels. Intermediate coupling calculations, as mentioned above, show a reduction of the $d_{5/2} \rightarrow \sigma_u$ intensity caused by exchange interaction; it corresponds to the fact that $d_{5/2}$-excitations correlate with singlet-triplet transitions in the limit of Russell-Saunders coupling.

Furthermore one should take into account, that in a single center expansion the $7\sigma_u$-orbital consists, besides the p_o component, of decreasing portions of f_o, h_o, ... AO's. This results in a reduction of the factor

$$f = \frac{|\langle d_1 | \underline{r} | \sigma_u \rangle|^2}{|\langle d_o | \underline{r} | \sigma_u \rangle|^2}$$

with the relative values of $|\langle \psi_1 | \underline{r} | \psi_2 \rangle|^2$ being

ψ_1 \ ψ_2	p_0	p_1	f_0	f_1
d_0	4	1	9α	6α
d_1	3	3	3α	8α
d_2	0	6	0	1α

below the value of 0.75 which tends to equalize the intensities of the two bands.

If a factor of f = 0.67 ($\sigma_u = p_0 + f_0$ with $\alpha = 0.1$) and a mean energy of $\varepsilon = -9.3$ eV is accepted for the upper level the calculated and measured spectra are almost identical as shown in the insert of Fig. 5 by the broken and solid lines, respectively. This would definitely not be the case if the ligand field were neglected, since this would lead to an identical width of both bands without any asymmetry, having an intensity ratio of exactly 1.5 : 1. As no further structure in the vicinity of the two peaks is observed it may be concluded that the 4d-5p exchange integral has indeed a negligibly small effect as presumed and theoretically justified above.

7. As far as the $7\sigma_u$-ε-value (point 7) is concerned it should be taken into consideration that the bands are Franck-Condon displaced. By using the approximate eq. (1) the vertical and adiabatic energy values can be estimated to be $\varepsilon_v \approx -9.3$ and $\varepsilon_a \approx -10.9$ eV. The latter value is to be compared with the Xe 5p ionization potential of ~12.5 eV. Whereas all the core levels are depressed by 3 eV, the $7\sigma_u$-level is raised by 1.5 eV. This latter phenomenon is attributed to the electrostatic and pseudo-potentials of the $F^{\delta-}$ entities, which will strongly interact with the $7\sigma_u$-electron.

4.2.2 The $4d \rightarrow 5p(8e_u)$ Transition in XeF_4

The discussion in the case of XeF_4 is complicated by the fact that the anti-bonding σ_u-orbitals of the two crossed F_2-molecules form an e_u-ligand orbital which mixes with the $5p_{\pm 1}$ Xe AO's. This has two consequences: 1. the e_u-level should exhibit a spin-orbit splitting and 2. coupling with non-totally symmetric vibrations should result in a Teller splitting of the degenerate electronic state.

The spin-orbit splitting of the e_u-orbital may be predicated as follows: the spin-orbit splitting of $5p^5\ ^2p\ Xe^+$ is known to be $\lambda = 1.31$ eV[20]. The spin-orbit coupling operator $-\frac{2}{3}\lambda\ \underline{L}\cdot\underline{S}$ in the basis set of the $p_{\pm 1}$ AOs has the eigensolutions

$$+0.44 \text{ eV} : |p_{+1}\alpha\rangle, |p_{-1}\beta\rangle \qquad (m_j = 3/2)$$

$$-0.44 \text{ eV} : |p_{-1}\alpha\rangle, |p_{+1}\beta\rangle \qquad (m_j = 1/2)$$

However, we do not know how much the $5p_{\pm 1}$ Xe AO contributes to the e_u-orbital. Basch et al.[9] calculated this to be 64 % in the virtual $8e_u$-orbital of the ground-state of XeF_4. This value can be expected to be too large because the cited computation overestimates the effective positive charge on the xenon atom. On the other hand, in the excited $(4d^9e_u)XeF_4$ state the e_u-orbital will be more localized near the xenon. (E.g. in the comparable case of the Cs^{2+} ion λ is 31 % larger.) We thus assume the molecular spin-orbit splitting to be near 0.6 - 0.7 eV.

If the e_u-orbital has a pure p-character the intensities of the $4d \rightarrow e_u$ $(m = \frac{1}{2})$ and $4d \rightarrow e_u (m = 3/2)$ transitions will be the same as those given in Column $I_{1/2}$ and $I_{3/2}$ of Table IV. This strongly suggests the assignment

given in Table V. If E_o and λ are chosen from the table to be -9.60 eV and 0.83 eV, respectively, an excellent agreement between the measured and calculated positions of the peaks is achieved. There is also fairly good agreement between the measured and calculated intensities. But due to the fact that the two peaks O'_{123} and O_{45} are measured to have a difference in half-width by a factor of 1.25, the more intense transition O'_{123} is measured to have a lower peaks height, which compares to the reversed behaviour in the case of the calculated curve (see insert of Fig. 6). We would like to make the following comments on these results:

1. The mean value for the energy E_o of the e_u-orbital is quite reasonable and thus leads to a vertical and an adiabatic energy of -9.6 eV and -11.2 eV, respectively. The somewhat higher energy in XeF_2, as compared to XeF_4, may be attributed to the higher effective charge of Xe in the latter compound. This corresponds to the computational result of Basch et al.[9] that the first virtual SCF-MO's are increasingly stabilized with increased fluorination.

2. The measured intensity of the 4d→5p-transition in XeF_4 is higher by a factor of 2.1 than in XeF_2. This is the expected relation because XeF_4 has two p-type final levels.

3. The first two peaks having $4d_{5/2}$ initial levels show a splitting of 1.15 eV, whereas the O_{45} peaks with the initial levels $4d_{3/2}$ are only separated by 0.75 eV. This apparent discrepancy in the effective spin-orbit splitting of the e_u-orbital originates in the ligand field splitting of the 4d-level. The values of Table V indicate that the ligand field strength chosen is of the right magnitude.

4. The effective e_u-spin-orbit splitting deduced from the measurements is 0.15 - 0.2 eV larger than the spin orbit splitting constant whose size is estimated on theoretical reasons. This difference should be attributed to a Jahn-Teller-effect in connection with the asymmetric b_{2g} stretching vibration of XeF_4 with ω = 502 K. In making some reasonable assumptions (enlargement of the F-F distance in the excited state by 1 a_o (see above) which means a Jahn-Teller distortion) one obtains an increase of the apparent spin-orbit splitting of about 0.2 eV[19].

5. Whereas the intensities of Table IV describe the measured absorption curve as being qualitatively correct, the quantitative agreement is not at the maximum: the peaks are not as different in height as predicted. However, as shown in the sixth column of Table V, the theoretical intensities are much better, if allowance is made for the dynamical Jahn-Teller effect[19].

4.3 Transitions into the 6s Molecular Rydberg Orbitals of XeF_2 and XeF_4

The systems 6s Cs, $5p^5 6s Xe$ and $5\pi_u^3\ 6s XeF_2$ are similar to the present ones. As they have ionization potentials between 3.8 and 3.9 eV[8,20], we expect the first Rydberg transitions for the two molecules in question as given in Table VI.

Among all transitions from the 4p level the 4p→6s one will be most intensive. Indeed, only the α peak is observed in the energy region below 180 eV. In ESCA-spectra the $4p_{1/2}$ level is exceptional as it gives rise, at most, to only a very weak and broad peak[10]. We are, therefore, not surprised that the corresponding transitions are not present in the absorption spectra.

The 4d→6s transitions are Laporte forbidden. In XeF_4 they are not observed. XeF_2, which exhibits a much more intense Rydberg spectrum, has two weak and broad bands, induced by vibronic coupling. From Table VI we deduce $\varepsilon_1 = -3.5$ eV and $\varepsilon_2 = -3.2$ eV. As in the case of the anti-bonding 5p orbital, the 6s Rydberg orbital has a higher energy the more fluorine atoms interact with it.

4.4 Transitions into the 6p-Rydberg Levels of XeF_2 and XeF_4

4.4.1 Transitions into the 6p-Rydberg Levels of XeF_2

The 6p-energy of Cs and Xe is 2.4 - 2.5 eV[10,13,20] with a spin orbit splitting of about 0.05 eV. The $4d_{3/2,\ 5/2} \rightarrow 6p$ transitions, therefore, appear in the 68 to 70 eV region. Six peaks are observed there: B_1, B_{23}, C_{23}, B_4, BC_{54}, C_5. The 6p Rydberg orbitals in XeF_2 are split by the action of the fluorine atoms. The p_{-1} orbitals lie lower than p_0 because the high effective positive charge of Xe is not shielded from the p_{+1} orbitals by the fluorine atoms. The spin-orbit splitting of the $p\pi$-orbital is negligibly small. With the energy values E_0 and $E_0 - \Delta$ for the $p\sigma$ and $p\pi$ levels we calculate the transitions and intensities of Table VII.

With regard to the intensities, we have to account for the fact that the $p\pi$ and $p\sigma$ orbitals differ in their radial parts. As the $p\pi$ orbital is contracted in comparison to the $p\sigma$ orbital, the quotient $c = |\langle 4d \mid \underline{r} \mid 6p\sigma \rangle|^2 \ / \ |\langle 4d \mid \underline{r} \mid 6p\pi \rangle|^2$ is smaller than unity.

With the parameters $E_0 = 2.45$ eV, $\Delta = 0.35$ eV, $c = 0.5$ and a natural line width of 0.25 eV for these dipoleallowed transitions into non-bonding orbitals, we obtain the broken line in Fig. 7.

The comparison between the measured and calculated spectrum leads to a few remarks: 1. The bands B_1, B_{23}, C_{23}, and BC_{54} are satisfactorily fitted, but the measured intensities of the bands B_4, and C_5 are definitely too high. This is attributed to transitions from the $4d_{5/2}$-levels into higher Rydberg orbitals (see Chapter 4.5). 2. As the initial and final state have the same non-bonding character the transitions should lead to relatively sharp peaks. In this case it will be possible to record splittings not only in the valence- and Rydberg orbitals but also in the core orbitals. Due to the non-totally symmetric ligand field the $4d_{5/2}$ core orbital splitting manifests itself in the 0.24 eV separation between the B_1 and B_{23} peaks, whereas the ligand field splitting of the $4d_{3/2}$ level is observed in the 0.31 eV gap between B_4 and BC_{54} and in the 0.36 eV gap between BC_{54} and C_5. This is, to our knowledge, the first time that splittings of inner levels by angular terms of a perturbing ligand field have been directly oberved.

4.4.2 Transitions into the 6p-Rydberg Levels of XeF_4

These transitions give rise to sharp peaks in the 70 - 73 eV region. In XeF_4, the $6p_o$ orbital is lower (by Δ) than the $6p_{\perp 1}e_u$ orbital which has an approximate energy of E_o = -2.5 eV. Table VIII shows the calculated excitation energies and related intensities. With E_o = -2.55 eV Δ = 0.45 eV and the same values for c and the line width as in XeF_2 we reproduce the measured spectrum as seen in Fig. 8. It has been explained in Chapter 3 why the C_4, C_5 peaks could not be identified with certainty.

As in the case of XeF_2 the ligand field results in an observable $4d_{5/2}$ level splitting which is recorded as an energy gap of 0.39 eV between

the two peaks C_1 and C_{23}. The splitting Δ in the final 6p level is larger than in XeF_2 due to the higher charge of Xe in XeF_4. The considerations carried out so far do not explain the lower intensity of the XeF_4 Rydberg spectrum as compared to the XeF_2 case. Evidently the fluorine atoms suppress by the combined influence of their negative charge and their pseudo-potentials, the penetration of the Rydberg orbitals into the Xe core[24].

4.5 Remaining Details of the Gaseous Spectra

In XeF_2 there are three further rather broad peaks with maxima at 70.89 eV (D), 71.47 eV (E) and 72.30 eV (F) which have not been discussed before. They lie in the strongly increasing $4d_{5/2}$ f-continuum[17] which starts at the $4d_{5/2}$ ionization energy of 70.5 eV. For energetic reasons these peaks must correspond to $4d_{3/2}$-excitations. The corresponding $4d_{5/2}$-excitations, which are 2 eV lower in energy, coincide with the $A_{1,5}$, B_4 and C_5 peaks at 69.0, 69.5 and 70.2 eV and lead to the missing intensity (Chapter 4.4.1). Quantum defect extrapolations for the 7p levels yield -1.25 eV. If we assign the D and E bands to the $4d_{3/2} \rightarrow 7p$ transitions this would imply $\varepsilon(7p\pi) = -1.45$ eV and $\varepsilon(7p\sigma) = -1.2$ eV. The corresponding $4d_{5/2} \rightarrow 7p$ transitions then cover the energy range from 68.8 to 69.55 eV and explain the left hand assymmetry of the B_4-band. The very broad and flat unresolved F-band and the excess intensity of the C_5-band are then due to excitations into higher molecular orbitals.

In XeF_4 only one broad peak (D) at 71.41 eV remains to be explained. It is well reproduced with the energy values -1.5 eV for $7p(a_{2u})$ and -1.3 eV for $7p(e_u)$. These values are just those to be expected from quantum defect extrapolations as well as from a comparison with Xe and XeF_2.

5. CONCLUSION

The absorption spectra of XeF_2 and XeF_4 measured in the 50 - 160 eV region show the continuous contribution from the F- and Xe-components and further a detailed structure which could be deduced as being due to transitions from the 4d Xe core into the lowest empty valence and Rydberg states of the molecules. The peak positions are measured with an accuracy of 0.1 eV whereas the relative intensities have an estimated error of 5 %. Within these limits of error a theoretical interpretation of the observed spectra has been given. This interpretation follows along the lines of the one-electron picture. The measured peak positions could be identified within a few hundredths of an eV by the differences of suitably adjusted one-electron levels. The level energies are given in Table IX.

The positions of the various absorption peaks are influenced by spin orbit splitting as well as by ligand field splitting. For the first time a core level splitting caused by the non-totally symmetric part of the ligand field is observed. The splittings are in the range of 1/4 to 1/2 eV and are smaller by a factor of nearly 2/3 than the computed values from SCF-calculations as given by Basch et al.[9]. This is the same factor as that between the chemical shifts from ESCA measurements and the level stabilization due to the symmetric part of the ligand field from these same SCF-calculations. In the case of XeF_4 a dynamic Jahn-Teller-effect[10] was found to exist. The interpretation of part of the structure as being due to Rydberg transitions is strongly supported by the fact that in the case of the solidified gases these transitions lead to very broad structures.

The MO's of Table IX correlate nicely with Xe AO's. The shift and the splitting of the 4d core orbitals and also of the higher Rydberg orbitals can be explained by the electrostatic model. But this is not possible for the shift of the $7\sigma_u$-LEMO and the lowest 6s Rydberg MO. These two orbitals overlap with the fluorine orbitals. The upward shift of the levels is explained as being caused by a repelling force which the fluorine ligands exert on these electrons according to pseudo-potential theory[23]. There is also a possibility of using the pseudo-potential of the fluorine atoms to explain the decreasing intensities of the Rydberg transitions by going from Xe to XeF_2 and XeF_4[24]. From this we do not expect that XeF_6 or $XeOF_4$ will show any detectable Rydberg transitions.

The comparison between the observed and calculated spectra (Fig.s 5 - 8) show excellent agreement for transitions into the LEMO and also for the Rydberg transitions in the case of XeF_2. The agreement is less but still good in the case of XeF_4. This is not surprisng if we remember that the one-electron picture and especially the two-dimensional harmonic oscillator potential used to calculate the vibronic spectra are rather rough approximations.

Acknowledgments

We wish to thank P. Habitz for his help in the computational part of the work. One of the authors (F.J.C.) is grateful to the DESY Board of Directors for making possible a five months' stay in Hamburg. Thanks are also due to the Deutsche Forschungsgemeinschaft for financial support.

References

1. N. Bartlett, Proc.Chem.Soc. 1962, 218 (1962)
   H.H. Claassen, H. Selig, and J.G. Malm, J.Am.Chem.Soc. 84, 3593 (1962)
   R. Hoppe, W. Dähne, H. Mattauch, and K.M. Rödder, Angew.Chem. 74, 903 (1962), Angew. Chem. Interntl. Ed. 1, 599 (1962)
2. H.H. Hyman, Ed., Noble Gas Compounds (Chicago University Press, Chicago, 1963)
3. J.G. Malm, H. Selig, J. Jortner, and S.A. Rice, Chem.Rev. 65, 199 (1965)
4. P.A. Agron, G.M. Begun, H.A. Levy, A.A. Mason, C.G. Jones, and D.F. Smith, Science 139, 842 (1963)
   S. Reichmann and F. Schreiner, J.Chem.Phys. 51, 2355 (1969)
5. S. Siegel and E. Gebert, J.Am.Chem.Soc. 85, 240 (1963)
   D.H. Templeton, A. Zalkin, J.D. Forrester, and S.M. Williamson, J.Am.Chem.Soc. 85, 242 (1963)
6. H.A. Levy and P.A. Agron, J.Am.Chem.Soc. 85, 241 (1963)
7. E.G. Wilson, J. Jortner, and S.A. Rice, J.Am.Chem.Soc. 85, 813 (1963)
   J. Jortner, E.G. Wilson, and S.A. Rice, J.Am.Chem.Soc. 85, 815 (1963)
   E.S. Pysh, J. Jortner, and S.A. Rice, J.Chem.Phys. 40, 2018 (1964)
   C.J. Eckhardt and G.D. Sturgeon, Chem.Phys. Letters 8, 300 (1971)
8. C.R. Brundle, M.B. Robin, and G.R. Jones, J.Chem.Phys. 52, 3383 (1970)
   B. Brehm, M. Menzinger and C. Zorn, Can.J.Chem. 48, 3193 (1970)
   C.R. Brundle, G.R. Jones, and H. Basch, J.Chem.Phys. 55, 1098 (1970)
9. H. Basch, J.W. Moskowitz, C. Hollister, and D. Hankin, J.Chem.Phys. 55, 1922 (1971)
10. K. Siegbahn, C. Nordling, G. Johansson, J. Hedman, P.F. Hedén, K. Hamrin, U. Gelius, T. Bergmark, L.O. Werme, R. Manne, and Y. Baer, ESCA Applied to Free Molecules (North-Holland, Amsterdam, 1969)
    S.E. Karlsson, K. Siegbahn, and N. Bartlett (to be published)

11. R. Haensel, G. Keitel, P. Schreiber, and C. Kunz, Phys. Rev. Letters 22, 398 (1969)
R. Haensel, G. Keitel, P. Schreiber, and C. Kunz, Phys. Rev. 188, 1375 (1969)
12. R. Haensel and C. Kunz, Z.Angew. Phys. 23, 276 (1967)
13. K. Codling and R.P. Madden, Phys. Rev. Letters 12, 106 (1964); Appl.Opt. 4, 1431 (1965)
14. R. Haensel, G. Keitel, U. Sonntag, C. Kunz, and P. Schreiber, phys.stat.sol. (a) 2, 85 (1970)
15. E.J. McGuire, Phys.Rev. 175, 20 (1968)
16. A.P. Lukirskii, I.A. Brytov, and T.M. Zimkina, Opt.Spektrosk. 17, 438 (1964) [English transl. Opt. Spectrosc. 17, 234 (1964)]
A.P. Lukirskii, I.A. Brytov, and S.A. Gribovskii, Opt.Spektrosk. 20, 368 (1966) [English transl. Opt.Spectrosc 20, 203 (1966)]
17. J.W. Cooper, Phys.Rev. Letters 13, 762 (1964)
U. Fano and J.W. Cooper, Rev.Mod.Phys. 40, 441 (1968)
D.J. Kennedy and S.T. Manson, Phys. Rev. A 5, 227 (1972)
18. P. Schreiber, thesis, Universität Hamburg 1970
G. Keitel, thesis, Universität Hamburg 1970
19. W.H.E. Schwarz and P. Habitz (to be published)
20. C.E. Moore, NBS Circular 467, III (Washington, 1958)
21. T.L. Gilbert and A.C. Wahl (unpublished results)
22. H.H. Claassen, C.L. Chernick, and J.G. Malm, J.Am.Chem.Soc. 85, 1927 (1963)
P. Tsao, C.C. Cobb, and H.H. Claassen, J.Chem.Phys. 54, 5247 (1971)
23. J.D. Weeks, A. Hazi, and S.A. Rice, Adv.Phys.Chem. 15, 283 (1969)
W.H.E. Schwarz, Theoret. Chem. Acta 11, 307 (1968)
24. J.L. Dehmer, J.Phys.Chem. 56, 4496 (1972)

Table I : Transition energies of XeF_2 in eV

peak	energy gas	energy solid	assignment
O_{23}	61.38	60.96	$4d_{5/2} \rightarrow 5p$
O_{45}	63.29	62.94	$4d_{3/2} \rightarrow 5p$
A_{123}	66.94	69.2	$4d_{5/2} \rightarrow 6s$
B_1	67.49		$4d_{5/2}(\delta_{5/2}) \rightarrow 6p\pi$
B_{23}	67.73		$4d_{5/2}(\pi_{3/2},\sigma_{1/2}) \rightarrow 6p\pi$
C_{23}	68.27		$4d_{5/2} \rightarrow 6p\sigma$
A_{45}	69.00	71.1	$4d_{3/2} \rightarrow 6s$ $\quad 4d_{5/2} \rightarrow 7p$
B_{45}	69.53		$4d_{3/2}(\delta_{3/2}) \rightarrow 6p\pi$
BC_{5L}	69.84		$4d_{3/2}(\pi_{1/2}) \rightarrow 6p\pi$ $4d_{3/2}(\delta_{3/2}) \rightarrow 6p\sigma$
C_5	70.20		$4d_{3/2}(\pi_{1/2}) \rightarrow 6p\sigma$
D	70.89	72.8	$4d_{3/2}(\delta_{3/2})$ $\quad 7p\pi$
E	71.47		$4d_{3/2}(\pi_{1/2})$ $\quad 7p\sigma$; $7p\pi$
F	72.30		$4d_{3/2} \rightarrow ?$
α	144.91	145.0	$4p_{3/2} \rightarrow 6s$

Table II : Transition energies of XeF_4 in eV

peak	energy	energy solid	assignment
O_{23}	62.85	62.68	$4d_{5/2} \rightarrow 5p(e_{1/2})$
O'_{123}	64.0	63.85	$4d_{5/2} \rightarrow 5p(e_{3/2})$
O_{45}	65.05	65.07	$4d_{3/2} \rightarrow 5p(e_{1/2})$
O_{45}	65.8	66.	$4d_{3/2} \rightarrow 5p(e_{3/2})$
B_{23}	69.88		$4d_{5/2} \rightarrow 6p(a)$
C_{23}	70.35		$4d_{5/2}(\pi_{3/2}, \sigma_{1/2}) \rightarrow 6p(e)$
C_1	70.74		$4d_{5/2}(\delta_{5/2}) \rightarrow 6p(e)$
D	71.41		$4d_{5/2} \rightarrow 7p(a,e)$
B_{45}	71.91		$4d_{3/2} \rightarrow 6p(a)$
C_5	72.62		$4d_{3/2} \rightarrow 6p(e)$
α	147.79		$4p_{3/2} \rightarrow 6s$

Table III : 4d-levels in XeF_2

level i	m_j	ψ	E(eV)	I
d_1	5/2	$\|d_2\alpha\rangle$	-70.2_6	0
d_2	3/2	$0.52\|d_2\beta\rangle + 0.85\|d_1\alpha\rangle$	-70.5_4	0.22
d_3	1/2	$0.66\|d_1\beta\rangle + 0.75\|d_0\alpha\rangle$	-70.7_2	0.36
d_4	3/2	$0.85\|d_2\beta\rangle - 0.52\|d_1\alpha\rangle$	-72.3_1	0.08
d_5	1/2	$0.75\|d_1\beta\rangle - 0.66\|d_0\alpha\rangle$	-72.6_6	0.34

Table IV : 4d-levels in XeF_4

level i	m_j ♯	ψ	E(eV)	$I_{1/2}$	$I_{3/2}$
d_1	5/2	$0.99\|d_2\alpha\rangle - 0.07\ d_{-2}\beta\rangle$	-73.2_7	0	0.59
d_2	3/2	$0.38\|d_2\beta\rangle + 0.92\|d_1\alpha\rangle + 0.06\|d_{-2}\beta\rangle$	-72.9_3	0.09	0.26
d_3	1/2	$0.61\|d_1\beta\rangle + 0.79\|d_0\alpha\rangle$	-72.8_2	0.18	0.06
d_4	3/2	$0.92\|d_2\beta\rangle - 0.38\|d_1\alpha\rangle - 0.03\|d_{-2}\beta\rangle$	-75.1_0	0.50	0.05
d_5	1/2	$0.79\|d_1\beta\rangle - 0.61\|d_0\alpha\rangle$	-74.8_1	0.23	0.04

♯ approximate quantum number

Table V : 4d→5p transition in XeF_4

peak	transitions	transition energy in eV calculated	transition energy in eV measured	relative intensities calculated without J.T.	relative intensities calculated with J.T.	relative intensities measured
O_{123}	$d_{123}\rightarrow e_u(\frac{1}{2})$	$72.85+E_o-\lambda/2=62.84$	62.8_5	0.27	0.35	0.48
O'_{123}	$d_{123}\rightarrow e_u(\frac{3}{2})$	$73.15+E_o+\lambda/2=63.97$	64.0_0	0.91	0.83	0.59
O_{45}	$d_{45}\rightarrow e_u(\frac{1}{2})$	$75.07+E_o-\lambda/2=65.06$	65.0_5	0.73	0.67	0.53
O'_{45}	$d_{45}\rightarrow e_u(\frac{3}{2})$	$75.01+E_o+\lambda/2=65.83$	$65._8$	0.09	0.15	0.4

Table VI : Transitions into the 6s Rydberg orbital

transitions: initial level(s)		transition energy in eV predicted	measured peak	
XeF_2	$4d_{5/2}$	$70.5 + \varepsilon_1 = 67.0$	A	66.94
	$4d_{3/2}$	$72.5 + \varepsilon_1 = 69.0$	A	69.00
	$4p_{3/2}$	$148.5 + \varepsilon_1 = 145.0$	α	144.91
	$4p_{1/2}$	$161 + \varepsilon_1 = 157.5$	-	
XeF_4	$4d_{5/2}$	$73.0 + \varepsilon_2 = 69.8$	-	
	$4d_{3/2}$	$75.0 + \varepsilon_2 = 71.8$	-	
	$4p_{3/2}$	$151 + \varepsilon_2 = 147.8$	α	147.79
	$4p_{1/2}$	$163.5 + \varepsilon_2 = 160.3$	-	

Table VII : Transitions into the 6p Rydberg orbitals of XeF_2

initial level	final level	calculated transition energy	calculated Intens.	assigned peak	measured peak maximum
d_1	$6p\pi_{1/2,3/2}$	$70.26+E_o-\Delta = 67.4_6$	1.0	B_1	67.49
d_2	$6p\pi_{1/2,3/2}$	$70.54+E_o-\Delta = 67.7_4$	0.6	B_{23}	67.73
d_3	$6p\pi_{1/2,3/2}$	$70.72+E_o-\Delta = 67.9_2$	0.4		
d_1	$6p\sigma$	$70.26+E_o = 67.8_1$	0.0·C		
d_2	$6p\sigma$	$70.54+E_o = 68.0_9$	0.35·C	C_{23}	68.27
d_3	$6p\sigma$	$70.72+E_o = 68.2_7$	0.6·C		
d_4	$6p\pi_{1/2,3/2}$	$72.31+E_o-\Delta = 69.51$	0.9	B_4	69.53
d_5	$6p\pi_{1/2,3/2}$	$72.66+E_o-\Delta = 69.82$	0.45	BC_{54}	69.84
d_4	$6p\sigma$	$72.31+E_o = 69.86$	0.15·C		
d_5	$6p\sigma$	$72.66+E_o = 70.21$	0.55·C	C_5	70.20

Table VIII : Transitions into the 6p Rydberg orbitals of XeF_4

initial level	final level	calculated transition energy[≠]	calculated intensity	assigned peak	measured peak maximum
$4d_3$	6pσ	69.81	0.6	$B_{2,3}$	69.88
$4d_2$	6pσ	69.94	0.4		
$4d_1$	6pσ	70.27	0.0	$C_{2,3}$	70.35
$4d_3$	6pπ	70.26	0.4·C		
$4d_2$	6pπ	70.39	0.6·C		
$4d_1$	6pπ	70.72	1.0·C	C_1	70.74
$4d_5$	6pσ	71.81	0.6	$B_{4,5}$	71.91
$4d_4$	6pσ	72.18	0.1		
$4d_5$	6pπ	72.26	0.4·C	C_4	-
$4d_4$	6pπ	72.63	0.9·C	C_5	72.62

[≠] $E_o = -2.55$, $\Delta = 0.45$ eV

Table IX : One electron energy levels (eV) in the system

$4d^9$ Xe $F_n^+ + e$ (n = 0, 2, 4)

level	Xe	XeF_2	XeF_4
$4d_{3/2}(\pi_{1/2})$	-69.52	-72.6_6	-74.8_1
$4d_{3/2}(\delta_{3/2})$		-72.3_1	-75.1_8
$4d_{5/2}(\sigma_{1/2})$	-67.55	-70.7_2	-72.8_1
$4d_{5/2}(\pi_{3/2})$		-70.5_4	-72.9_4
$4d_{5/2}(\delta_{5/2})$		-70.2_6	-73.2_7
5p	(-12.5)[a]	-9.3_0 ($-10._9$)[b] $7\sigma_u$	-10.0 ($-11._6$)[b] $8e_{u1/2}$
			-9.2_8 ($-10._8$)[b] $8e_{u3/2}$
6s	- 3.8	- 3.5	- 3.2
6p	- 2.46	-2.8_0 (π_u)	-3.0_0 (a_{2u})
		-2.4_5 (σ_u)	-2.5_5 (e_u)
7p	- 1.18	-1.4_5 (π_u)	- 1.5 (a_{2u})
		-1.2 (σ_u)	- 1.3 (e_u)
ionization limit [c]	0.00	0.0 ± 0.2	0.0 ± 0.2

a) Mean ionization potential of Xe

b) Adiabatic energy value

c) Corresponding to Siegbahn's ESCA-measurements

Figure Captions

Fig. 1 Experimental set-up. EO = electron-orbit, V = valve, BS = beam shutter, GPM = plane mirror, CH = chopper wheel, GC = gas-cell, CR = cryostat, CM = concave mirror, G = grating, PM = photo-multiplier, RA = rotating arm

Fig. 2 Sample chamber used for the measurements of the gaseous and solidified xenon fluorides

Fig. 3 Absolute cross-section of gaseous and solid XeF_2 (solid curves) and Xe (dashed curve) versus photon energy in the energy range of 50 - 160 eV

Fig. 4 Absolute cross-section of gaseous and solid XeF_4 versus photon energy in the energy range of 50 - 160 eV

Fig. 5 Absolute cross-section of gaseous (——) and solid (· — · —·) XeF_2 versus photon energy in the energy range of 60 - 75 eV. Insert: measured (——) and calculated (----) relative cross-section of gaseous XeF_2 in region b (60 - 65 eV)

Fig. 6 Absolute cross-section of gaseous (——) and solid (·—·—·) XeF_4 versus photon energy in the energy range of 61 - 72 eV. Insert: measured (——) and calculated (-----) relative cross-section of gaseous XeF_4 in region b (62 - 67 eV)

Fig. 7 Measured (——) and calculated (----) cross-section of XeF_2 in region c (66 - 73 eV)

Fig. 8 Measured (——) and calculated (----) cross-section of XeF_4 in region c (69 - 72.5 eV)

Fig. 9 Fluorine ligand field splitting of the 4p and 4d Xe AO's in XeF_2 and XeF_4

Fig. 10 4d level splitting in XeF_2 by ligand field ($V_{lig} \neq 0$, $\lambda = 0$), by spin-orbit interaction ($V_{lig} = 0$, $\lambda \neq 0$), and by both effects

Fig. 11 4d level splitting in XeF_4 by ligand field ($\lambda = 0$), by spin-orbit interaction ($V_{lig} = 0$), and by both effects

Fig. 12 4p level splitting and wave functions in XeF_2 and XeF_4 by spin-orbit interaction and a relatively small additional ligand field.

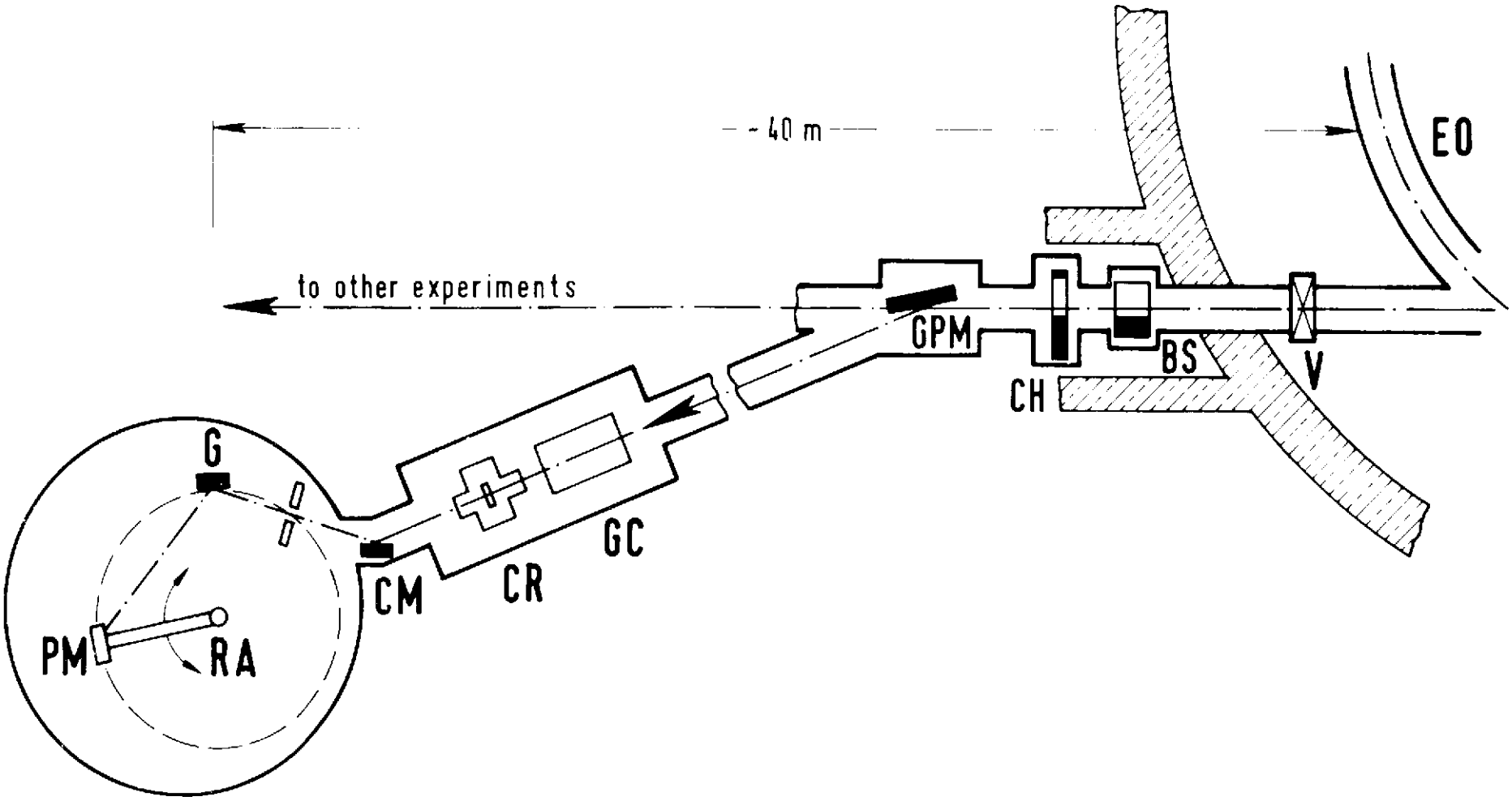

Fig.1

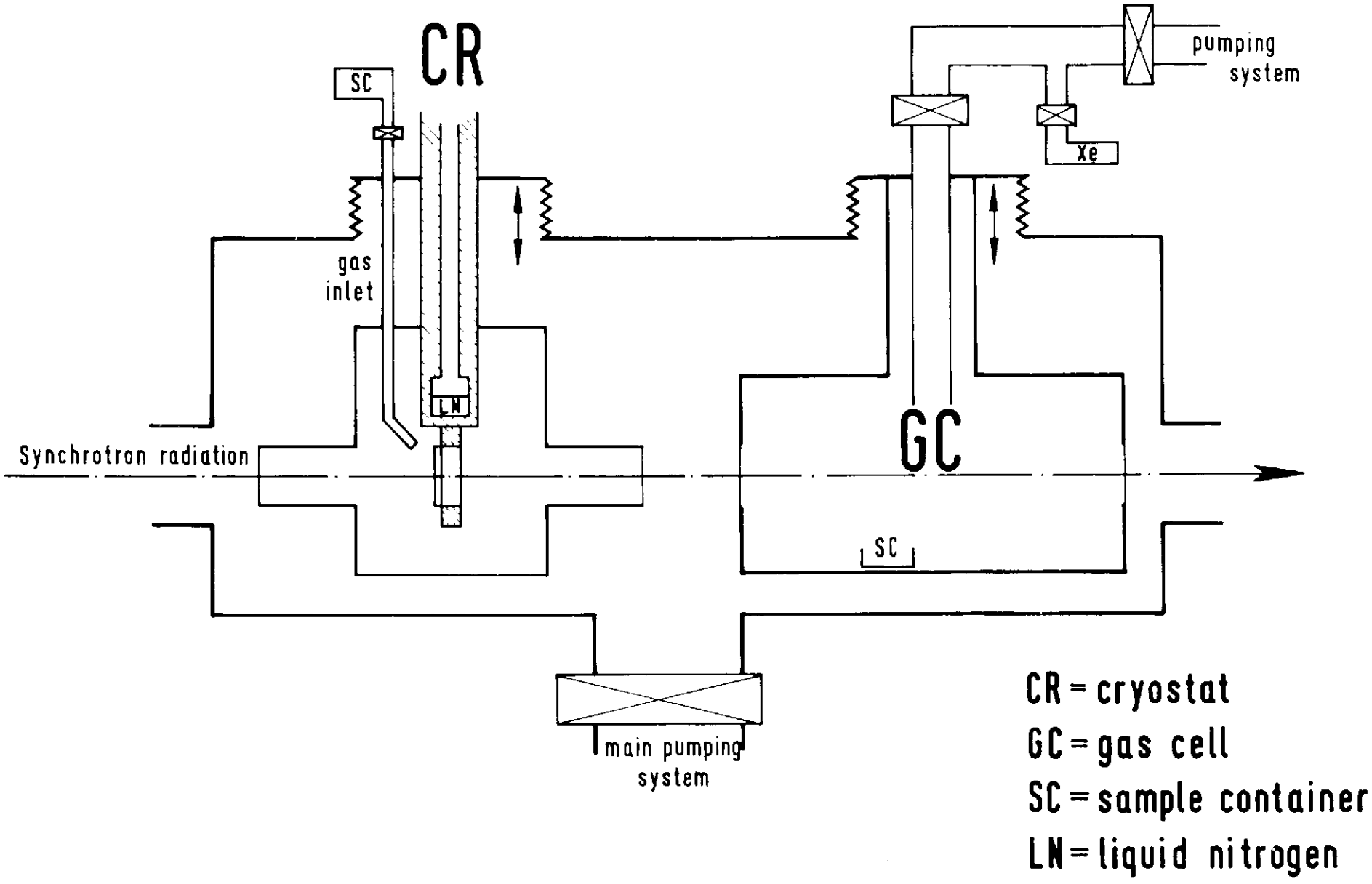
CR
SC
pumping system
Xe
gas inlet
LN
GC
Synchrotron radiation
SC
main pumping system
CR = cryostat
GC = gas cell
SC = sample container
LN = liquid nitrogen

Fig. 2

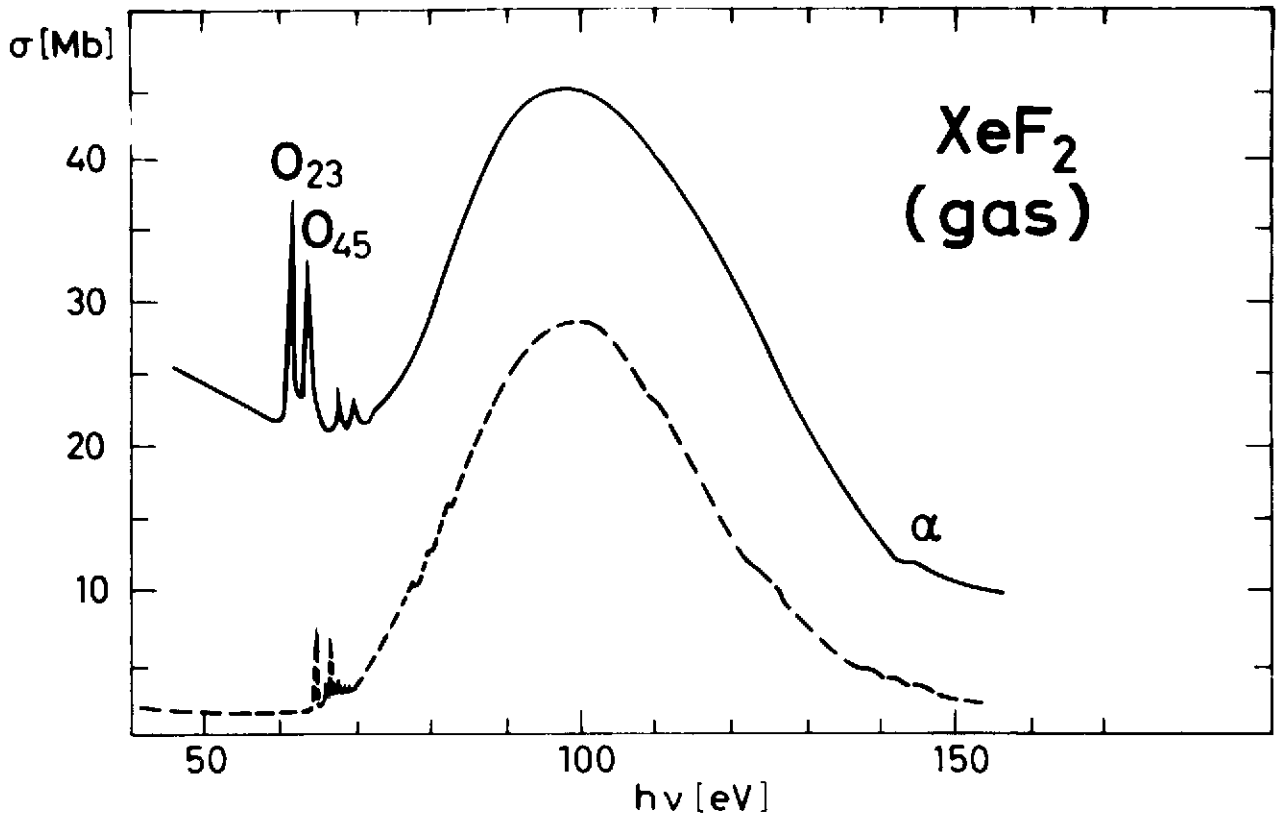
σ [Mb]
40
30
20
10
O23
O45
XeF2
(gas)
α
50
100
150
hν [eV]

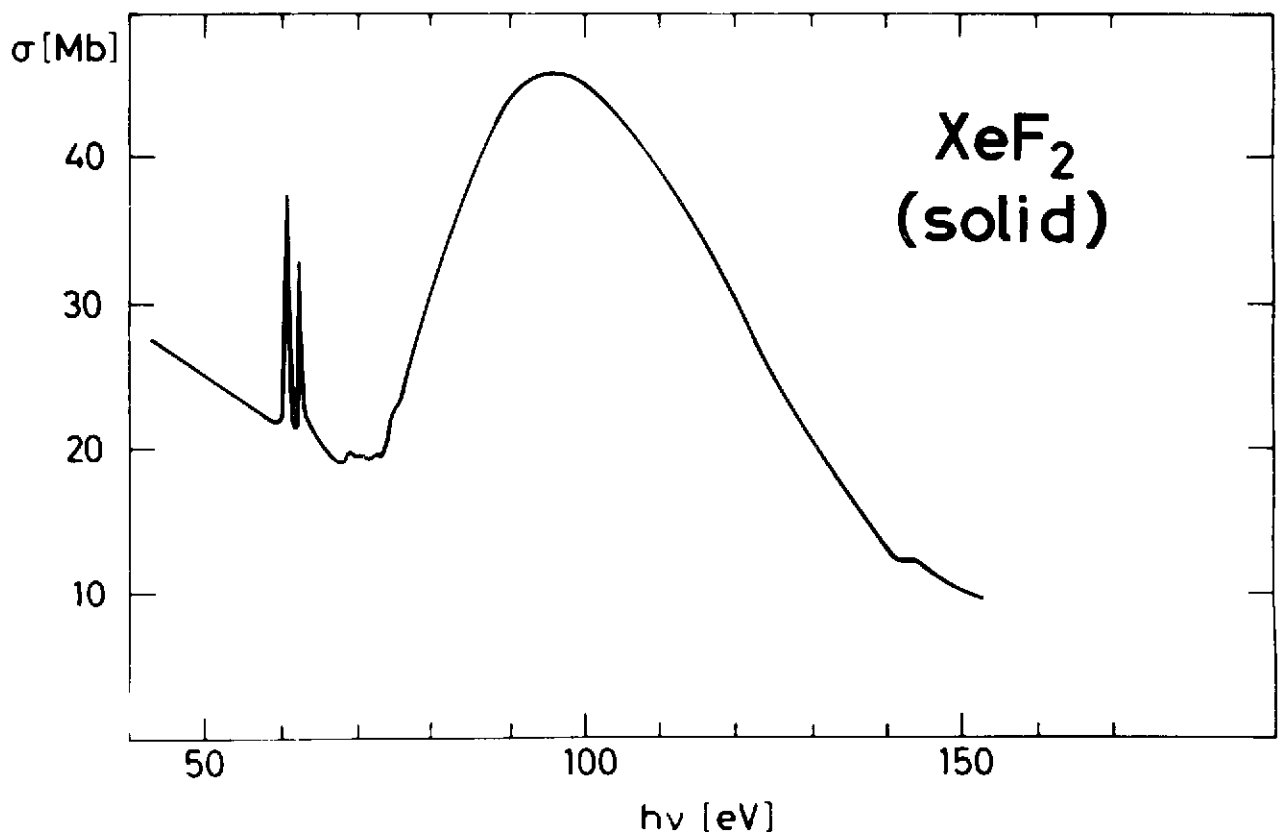
σ [Mb]
40
30
20
10
XeF2
(solid)
50
100
150
hν [eV]

Fig.3

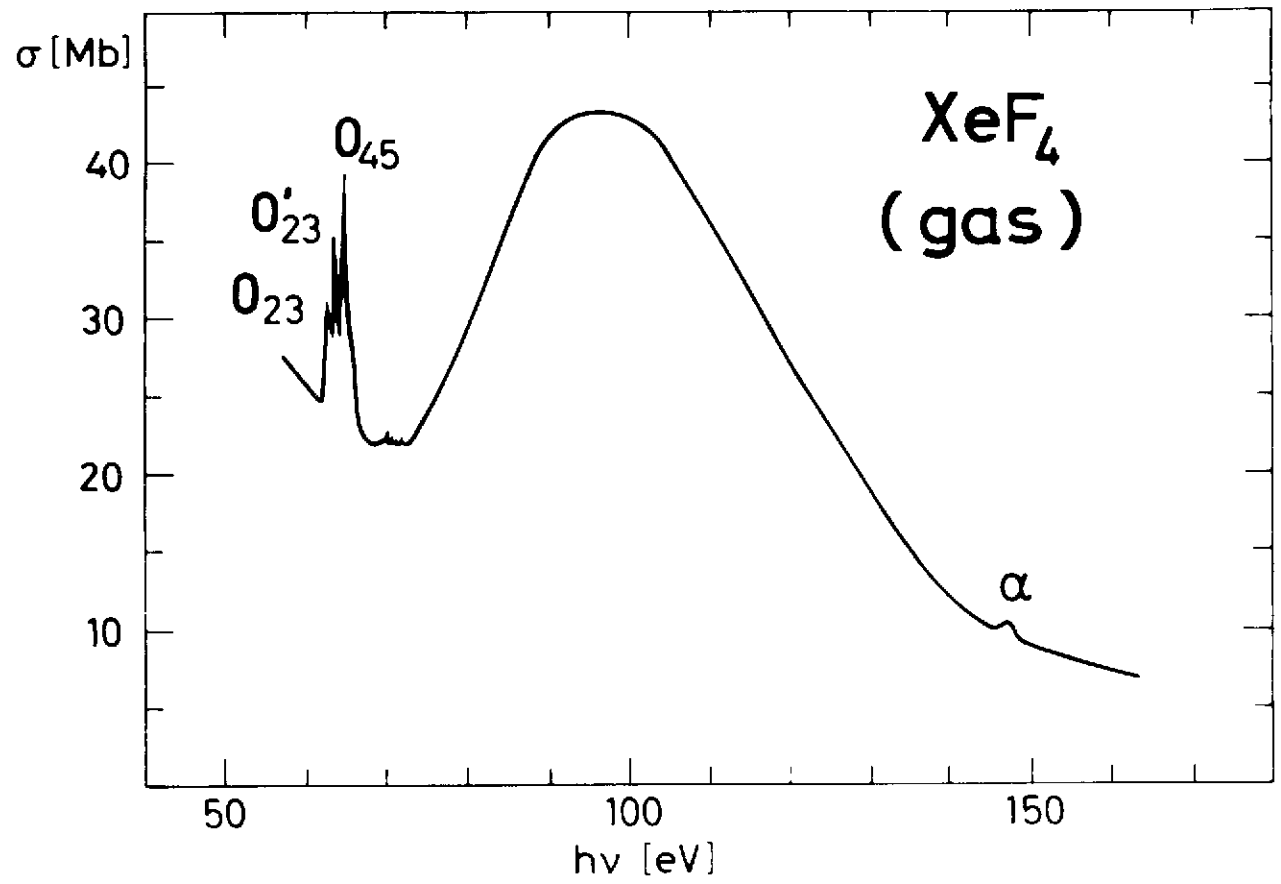
σ [Mb]
40
30
20
10
O_{45}
O'_{23}
O_{23}
XeF_4
(gas)
α
50
100
150
hν [eV]

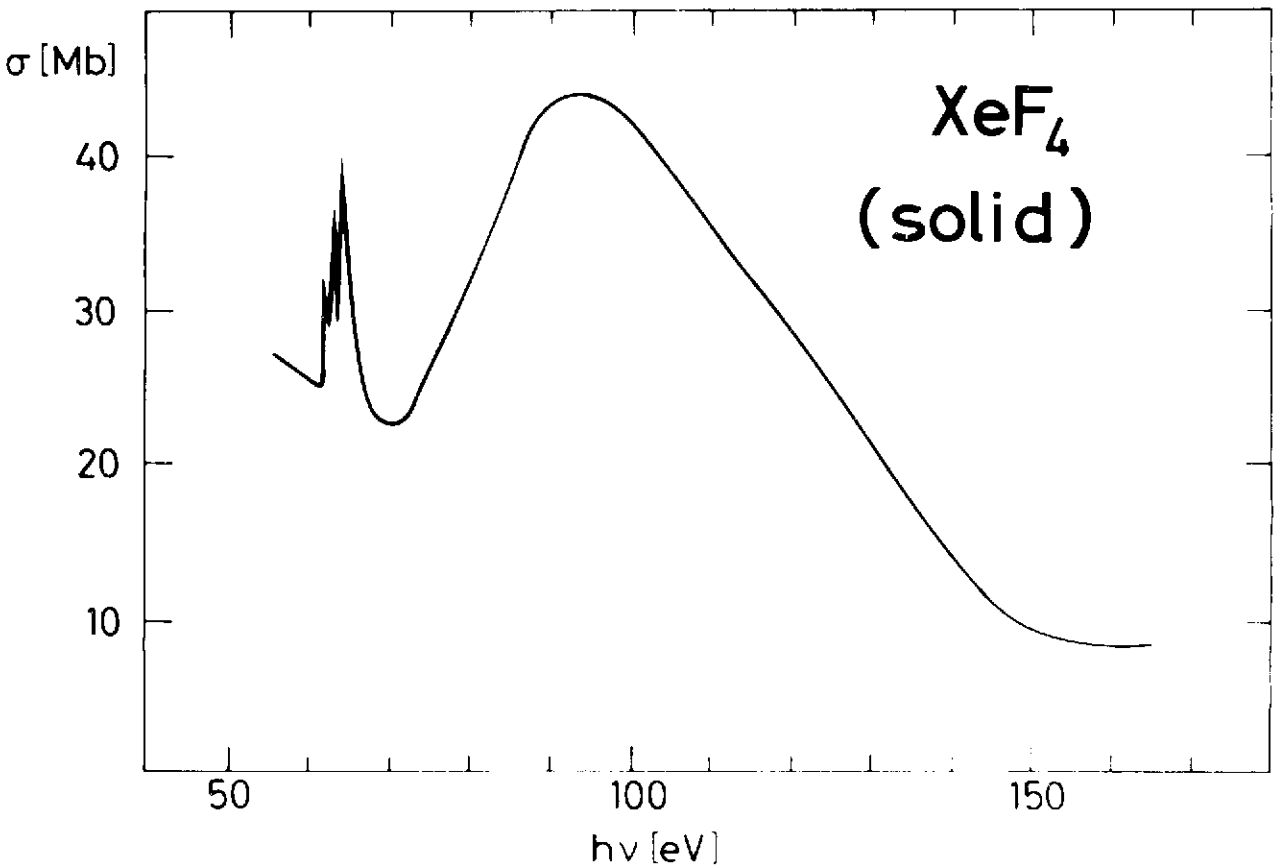
σ [Mb]
40
30
20
10
XeF_4
(solid)
50
100
150
hν [eV]

Fig. 4

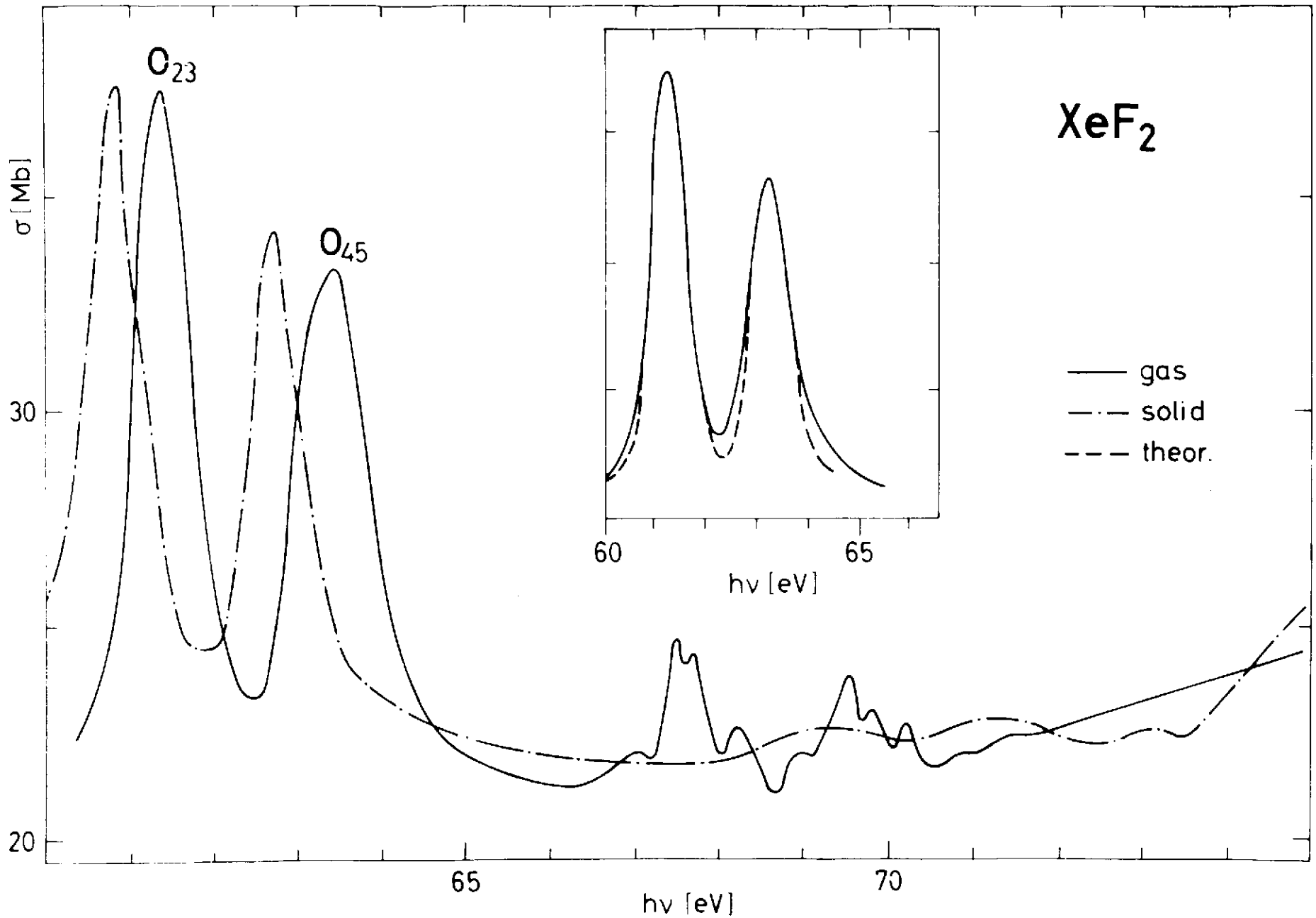

Fig.5

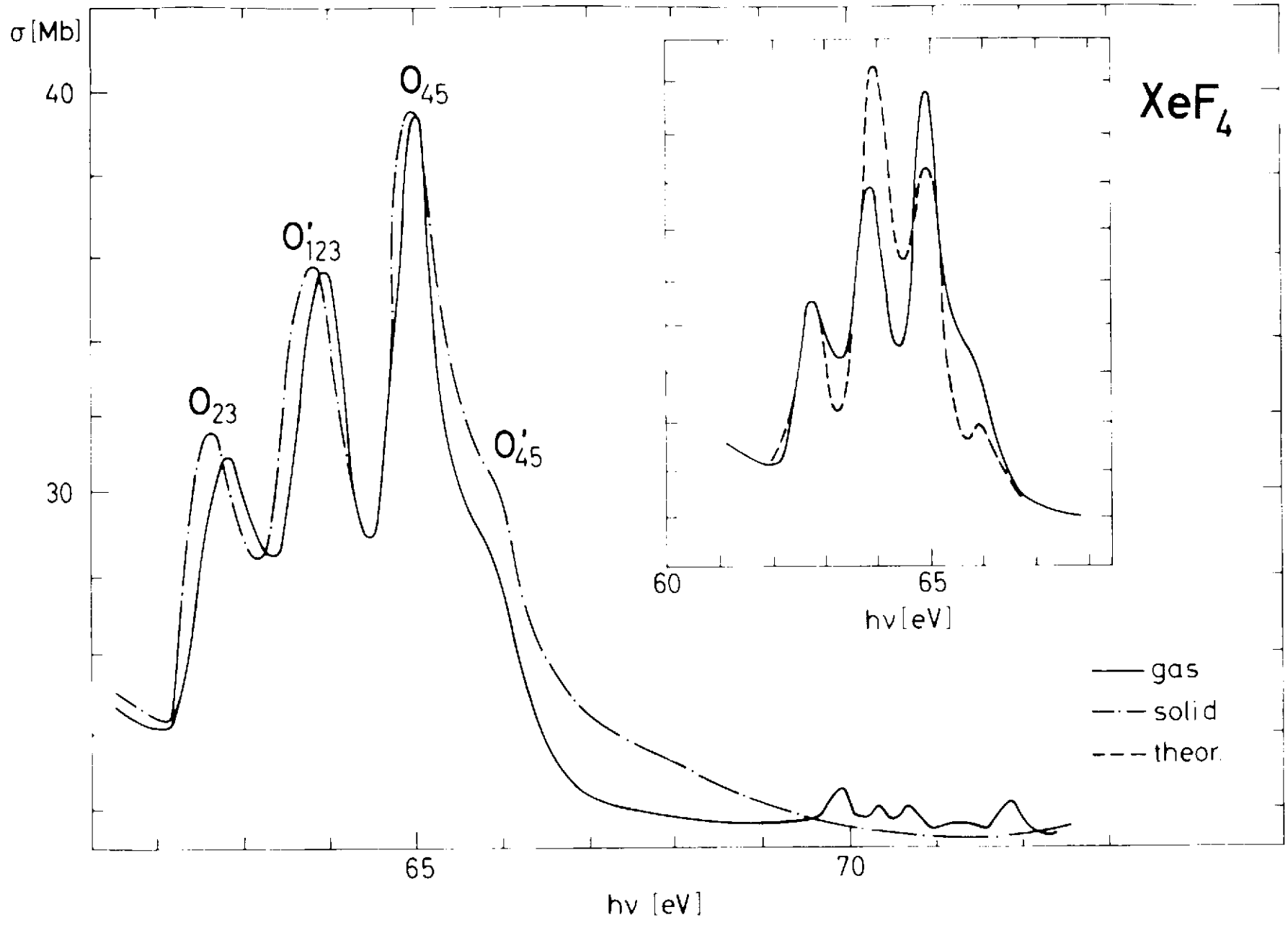
σ [Mb]
40
30
O_{45}
O'_{123}
O_{23}
O'_{45}
65
70
hν [eV]
60
65
hν [eV]
XeF_4
gas
solid
theor.

Fig.6

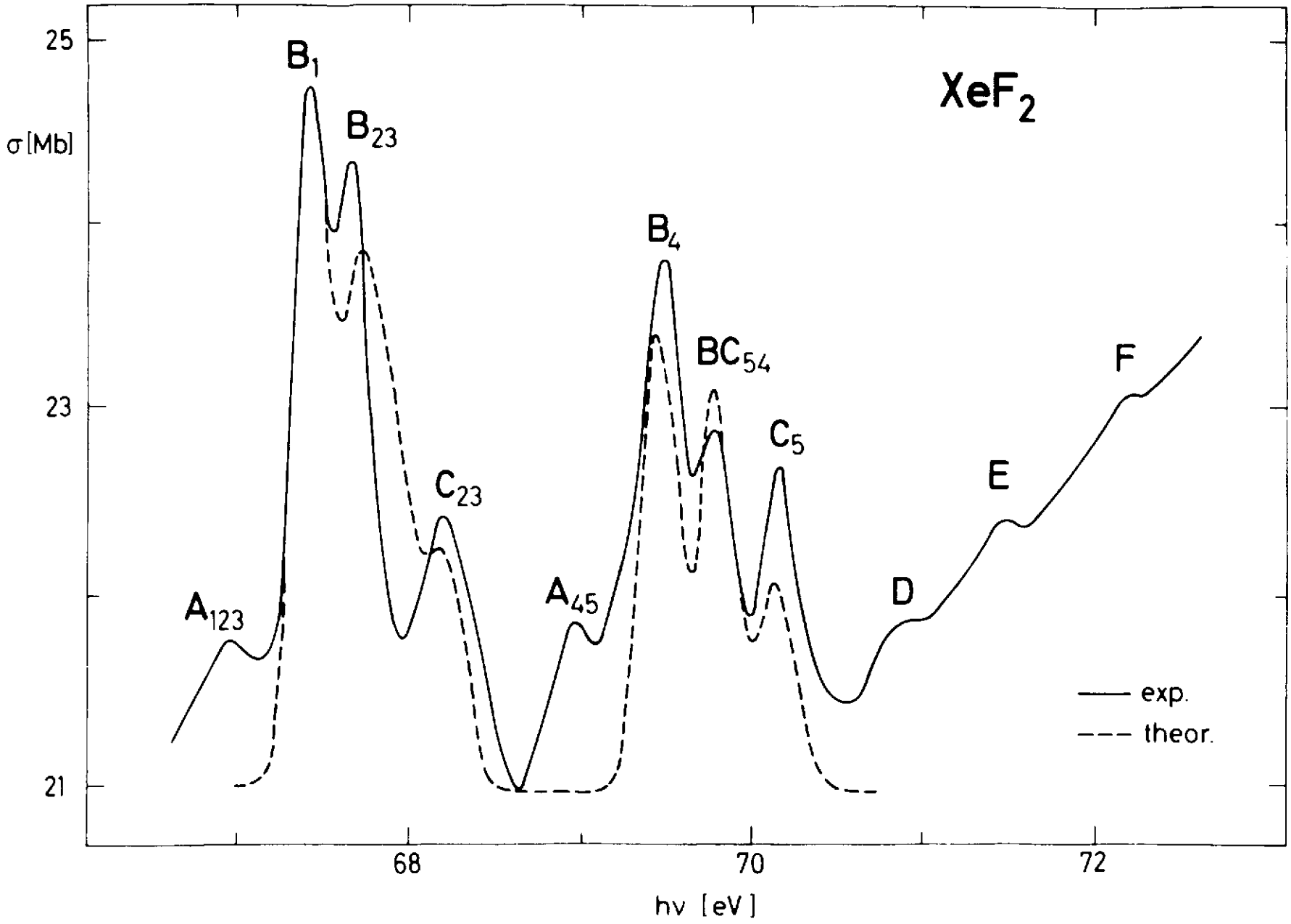
25
23
21
σ [Mb]
B1
B23
B4
BC54
C5
C23
A123
A45
D
E
F
XeF2
exp.
theor.
68
70
72
hν [eV]

Fig. 7

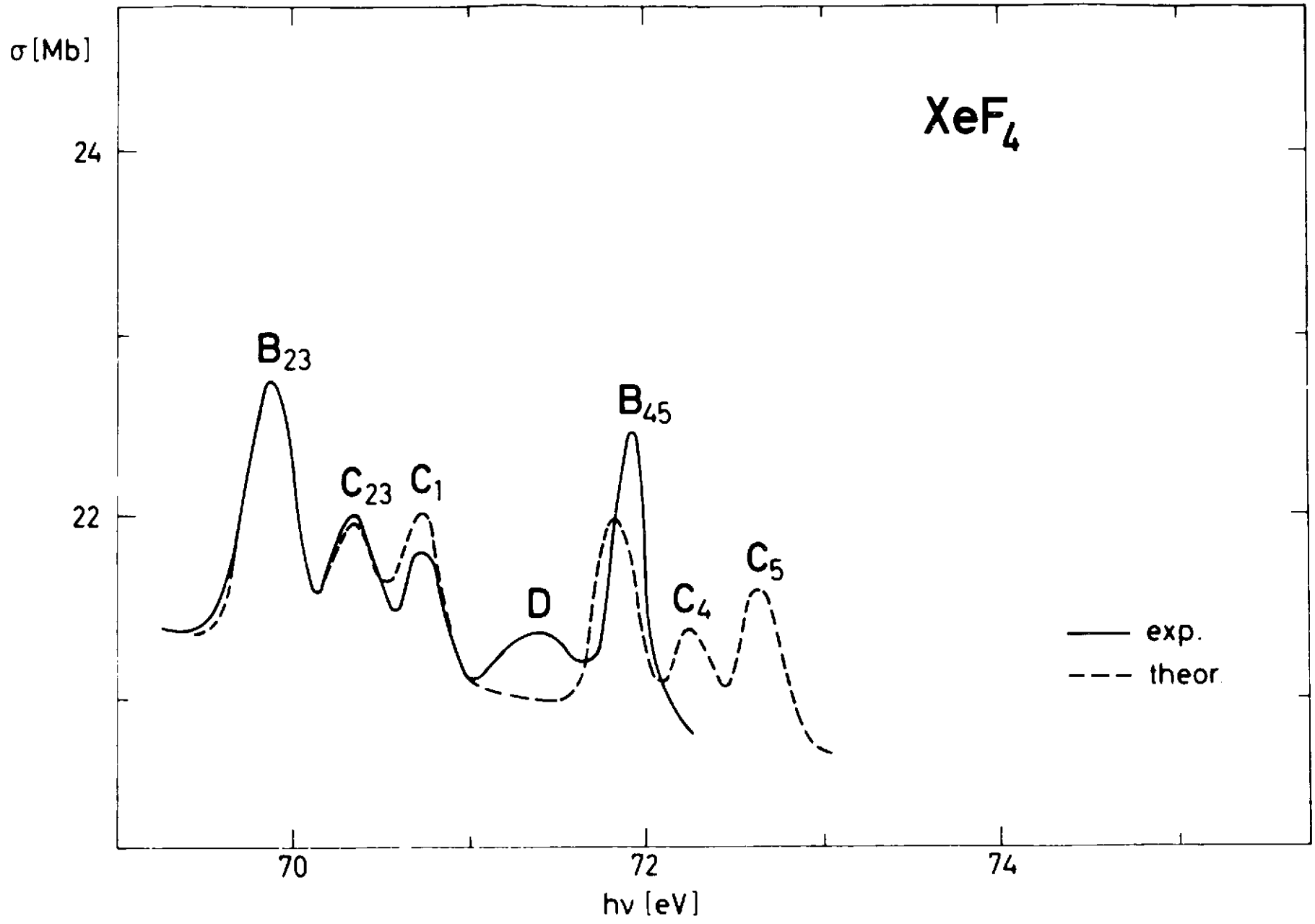

Fig. 8

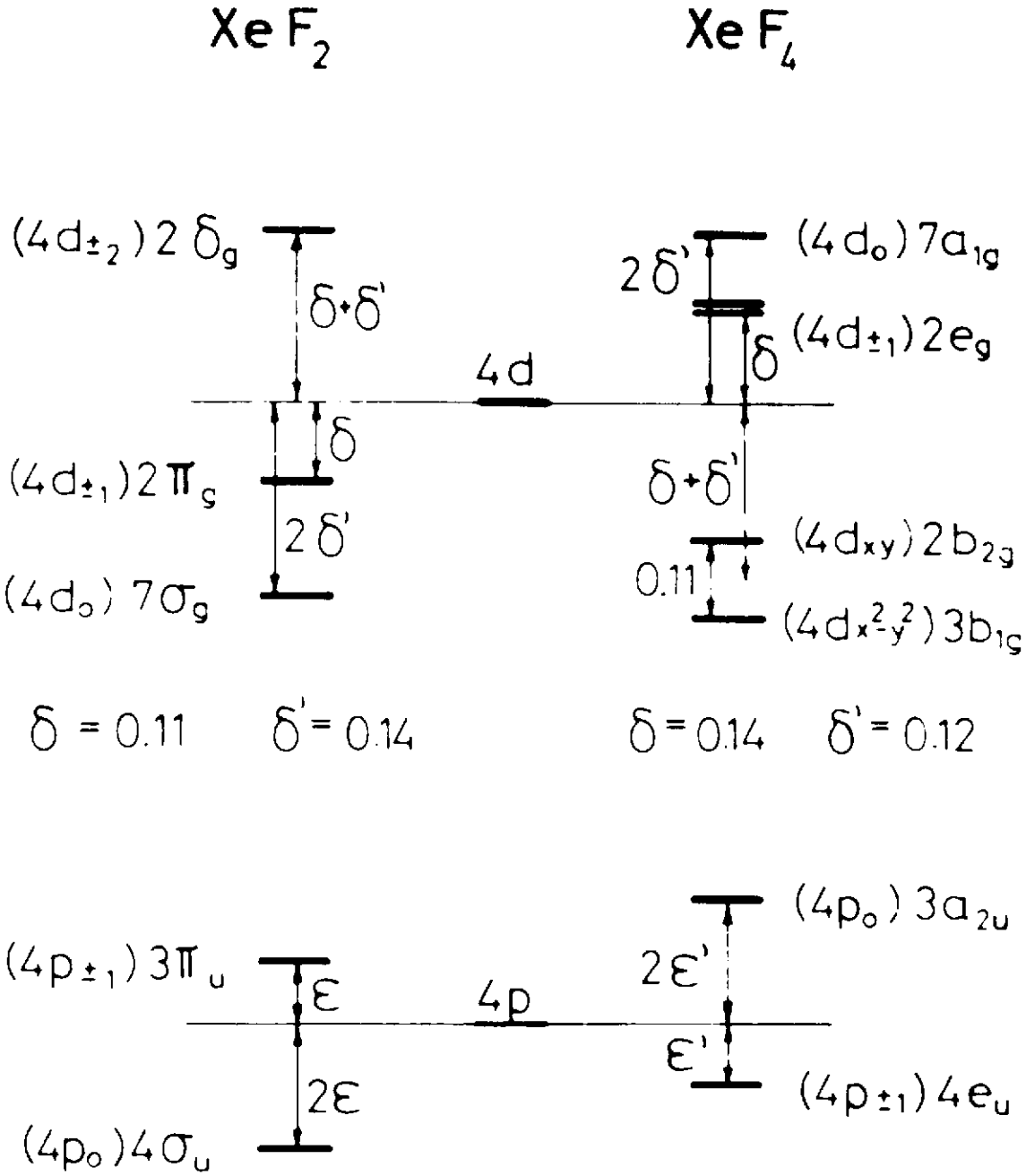
XeF2
XeF4
(4d±2) 2δg
δ+δ'
4d
δ
(4d±1) 2πg
2δ'
(4do) 7σg
2δ'
(4do) 7a1g
δ
(4d±1) 2eg
δ+δ'
(4dxy) 2b2g
0.11
(4dx2-y2) 3b1g
δ = 0.11
δ' = 0.14
δ = 0.14
δ' = 0.12
(4p±1) 3πu
ε
4p
2ε
(4po) 4σu
(4po) 3a2u
2ε'
ε'
(4p±1) 4eu
ε = ε' = 0.09

Fig. 9

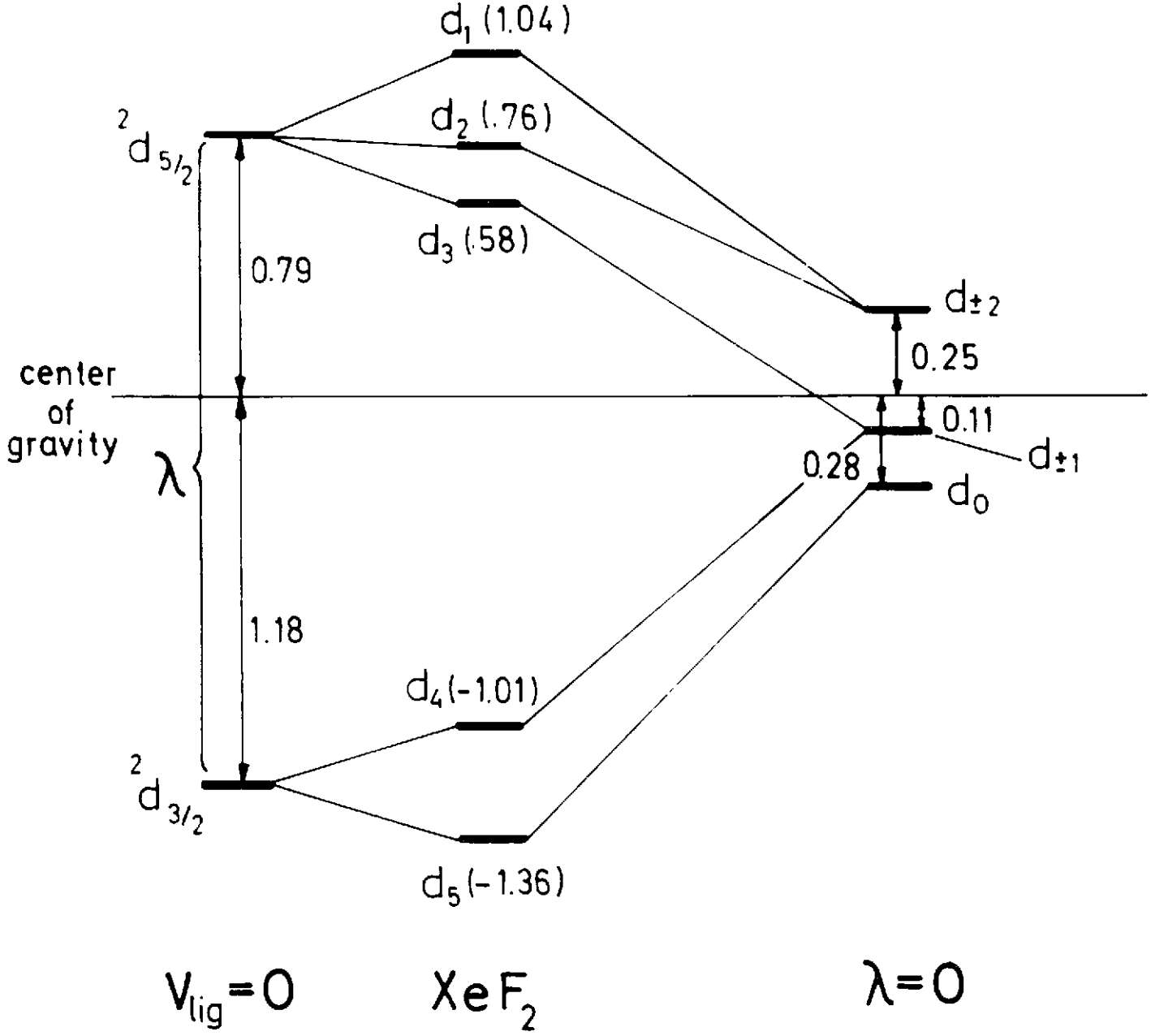
d_1 (1.04)
d_2 (.76)
$^2d_{5/2}$
d_3 (.58)
0.79
$d_{\pm 2}$
0.25
center of gravity
0.11
$d_{\pm 1}$
λ
0.28
d_0
1.18
d_4(-1.01)
$^2d_{3/2}$
d_5(-1.36)
$V_{lig}=0$
XeF_2
λ=0

Fig.10

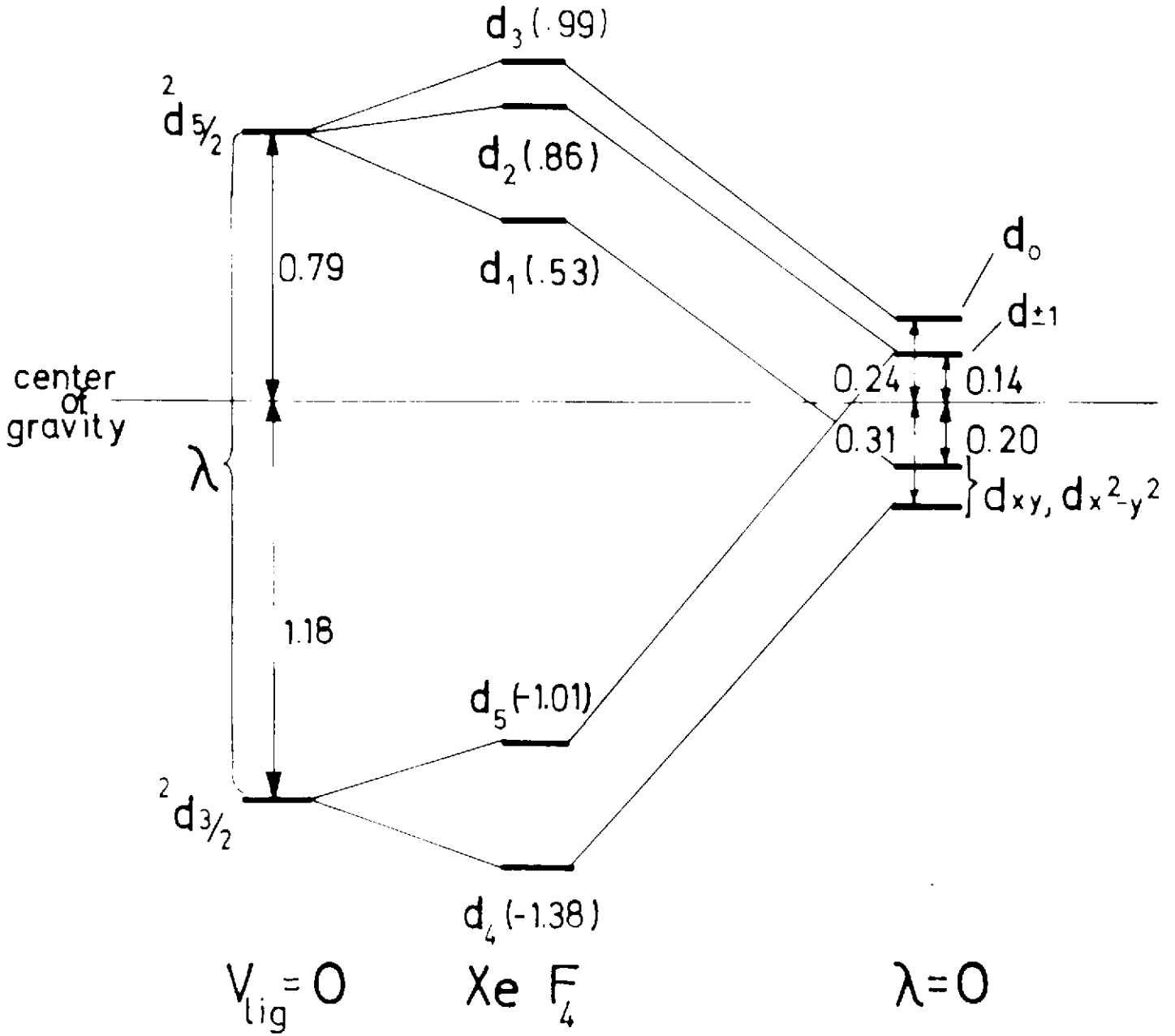
d_3 (.99)
$^2d_{5/2}$
d_2 (.86)
d_1 (.53)
0.79
d_o
$d_{\pm 1}$
center of gravity
0.24
0.14
0.31
0.20
$d_{xy}, d_{x^2-y^2}$
λ
1.18
d_5 (-1.01)
$^2d_{3/2}$
d_4 (-1.38)
$V_{lig} = 0$
Xe F_4
λ=0

Fig.11

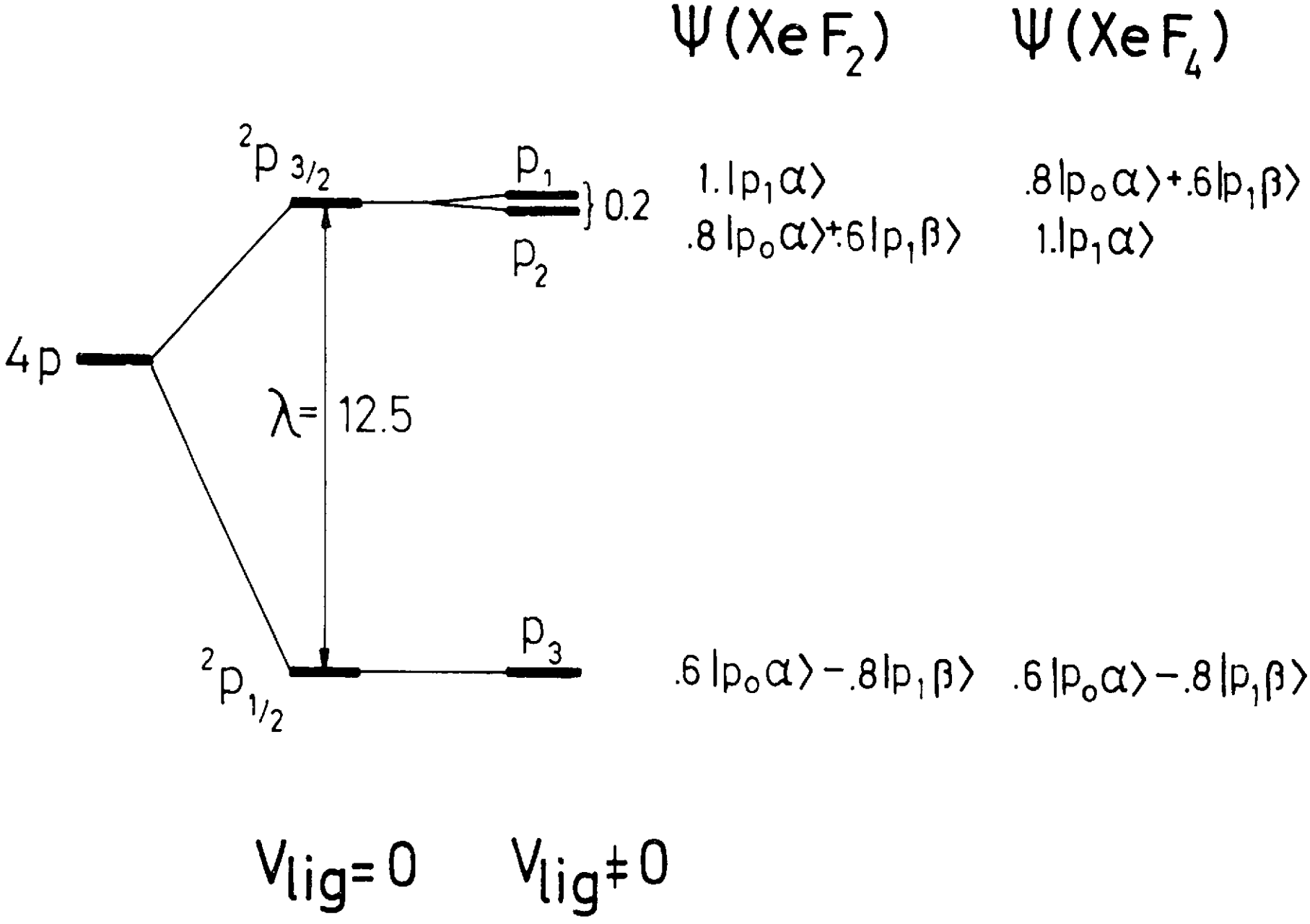
Ψ(XeF2)
Ψ(XeF4)
2P 3/2
P1
0.2
P2
4p
λ= 12.5
P3
2P 1/2
1.|p1α⟩
.8|p0α⟩+.6|p1β⟩
.8|p0α⟩+.6|p1β⟩
1.|p1α⟩
.6|p0α⟩−.8|p1β⟩
.6|p0α⟩−.8|p1β⟩
Vlig=0
Vlig≠0

Fig.12